INSTITUTE OF HIGH-ENERGY PHYSICS, SERPUKHOV

Report IHEP OP/SPK 70-93

FOCUSING DEVICE FOR NEUTRINO EXPERIMENTS

V.I. Voronov, I.A. Danil'chenko,
R.A. Rzaev and A.V. Samojlov

Serpukhov 1970

Translated at CERN by R. Luther
(Original: Russian)
Revised by N. Mouravieff

(CERN Trans. 72-19)

Geneva
November 1972

1. Introduction

In solving various problems encountered in elementary particle physics, and in particular in neutrino experiments, one has to convert a divergent beam of charged particles into a parallel or quasi-parallel beam over the widest possible energy and angle range. When these conditions are fulfilled, the neutrino flux produced from the decay of π-and K-mesons will be at a maximum. It is also important to carry out the conversion over as short a distance as possible, so that there is still a significant part of the decay length available for the beam.

Up until now, the following systems have been used or examined for this purpose: a magnetic horn[1], a plasma lens[2], magnetic fingers[3] and a horn with one or two additional reflectors[4]. With these systems, an axisymmetric magnetic field is excited by a pulsed current of several hundred kiloamp.

The distinctive feature of devices[1,3,4] is that they can only produce a parallel beam of neutrino parents (NP) in the following cases: a) NP momentum fixed, production angles arbitrary; b) NP production angle fixed, momenta arbitrary. The NP is focussed satisfactorily by these systems for any momentum and production angle by finding an acceptable compromise between the above limiting cases. This is done by selecting the geometry of the current-carrying shells according to the assumption concerning the shape of the angular and momentum spectrum of the NP. One of the main values defining the focussing properties of the system is the function

$$F = \frac{\alpha_{\text{entr.}}}{\alpha_{\text{emiss.}}}, \qquad (1)$$

where $\alpha_{\text{entr.}}$ is the entrance angle of the particles into the focussing system and $\alpha_{\text{emiss.}}$ is the emission angle.

In general the F value is a function both of the particle's

momentum and its production angle. To illustrate this, Fig. 1 shows a graph of the function $F = F(\alpha_{entr.}, p)$ for one of the horns[5].

For the plasma lens[2] the dependence of focussing on $\alpha_{entr.}$ is negligible although, as with systems[1,3,4], its dependence on the momentum of the NP is fairly great.

We also studied the focussing properties of various systems comprising linear-focussing elements, that is lenses with a deflecting force directly proportional to their radius r (in a thin-lens approximation):

$$Bz = cr, \tag{2}$$

where c = const., and z is the unit's length. Such fields may be set up, for example, by the following devices:

1) a plasma lens which consists of a current-carrying plasma filament enclosed within an outer sheath of revolution. If the current is distributed uniformly across the filament, the deflecting force of the lens has the form (2).

2) a parabolic lens which consists of two metal paraboloids of revolution joined at the vertices[6]. A magnetic field is set up in the space between the paraboloids through which the pulsed current passes (fig. 2). The lens length equals:

$$z = br^2, \; b = \text{const.} \tag{3}$$

The field component in the lens:

$$B\varphi = B = \frac{a}{r}, \; a = \text{const.} \tag{4}$$

2. STUDY OF MULTILENS SYSTEMS IN A THIN-LENS APPROXIMATION

1. Reference equations

Let us consider a random system comprising n thin lenses (Fig. 3), and take as parameters of the system the strengths of the lenses x_j and the distances between the (j-1)-th and the j-th lenses ℓ_j. With these designations, ℓ_1 is the distance from the NP source to the centre of the first lens. We now introduce the dimensionless units:

$$x_j' = \frac{x_j \ell_1}{p_o}, \qquad \ell_j' = \frac{\ell_j}{\ell_1}, \qquad p' = \frac{p}{p_o}, \tag{5}$$

where p is the particle's momentum and p_o is the scale factor. From now on, we shall only use the (5) units in our calculations and therefore the dashes will be omitted.

The matrix of the T system, consisting of n lenses, takes the form:

$$T = M_n L_n M_{n-1} L_{n-1} \cdots M_j L_j \cdots M_1 L_1. \tag{6}$$

Here M_j are the lens matrices and L_j the matrices of the free gaps preceding them.

In a thin-lens approximation

$$M_j = \begin{bmatrix} 1 & 0 \\ \frac{-x_j}{p} & 1 \end{bmatrix}, \qquad L_j = \begin{bmatrix} 1 & \ell_j \\ 0 & 1 \end{bmatrix} \tag{7}$$

The focussing function in this system coincides with the element of the T_{22} matrix. From (6) and (7) it can be seen that T_{22} is proportional to the polynomial of the nth power in terms of p, i.e.

$$F_n(p) = \frac{\alpha_{\text{ВЫХ}}}{\alpha_{\text{ВХ}}} = T_{22}(p) = \frac{1}{p^n}\left[p^n - R_1 p^{n-1} + R_2 p^{n-2} - \ldots + (-1)^n R_n\right]. \tag{8}$$

The R_j coefficients depend on the parameters of the $\{x, \ell\}$ system. The NP beam is focussed in parallel if the condition $\alpha_{emiss.}(p) \equiv 0$ is fulfilled throughout the momentum range, i.e. $F_n(p) \equiv 0$.

In fact the polynomial in (8) only becomes zero for certain momentum values $p_1, p_2, \ldots p_k$, $k \leqslant n$, which are its roots:

$$\begin{cases} F_n(x, \ell/p_1) = 0, \\ F_n(x, \ell/p_2) = 0, \\ \ldots\ldots\ldots\ldots \\ F_n(x, \ell/p_n) = 0. \end{cases} \tag{9}$$

If the conditions of (9) are met for momenta p_1, p_2,... p_k, lying within the working range $p_{min} \div p_{max}$, then, by increasing the number of lenses and, consequently, of momenta extracted in parallel, focussing in that range will be improved. Fig. 4 illustrates the variation in focussing in a range for which $\frac{p_{max}}{p_{min}} = 4$ when the number of roots in it is increased. The curves correspond to cases where n = 1, 2, 3, 5.

We note that if certain roots p_n, $p_{n-1}, \ldots, p_{n-k} \ll p_{min}$, then the behaviour of $F_n(p)$ in the range $p_{min} \div p_{max}$ is virtually independent of these roots. In fact, in this range, the following is valid up to the value $\frac{p_{n-k}}{p_{min}}$:

$$F_n(p) = \left(1 - \frac{p_1}{p}\right)\left(1 - \frac{p_2}{p}\right) \ldots \left(1 - \frac{p_n}{p}\right) \approx \left(1 - \frac{p_1}{p}\right) \ldots \left(1 - \frac{p_{n-k}}{p}\right) = F_{n-k}(p). \tag{10}$$

Therefore, it is only worth increasing the number of roots and hence the number of lenses in the system as long as the roots can be placed within or close to the range $p_{min} \div p_{max}$ without violating the conditions of (9) at real values of the parameters $\{x, \ell\}$.

Let us obtain the conditions of (10) in an explicit form.

If we denote

$$\sum_{k=i+1}^{j} \ell_k = s_{ij} ,$$

then the R_j coefficients can be recorded in terms of X_j and ℓ_j as follows:

$$\begin{cases} R_1(x,\ell) = \sum_{i=1}^{n} x_i s_{0i} , \\ R_2(x,\ell) = \sum_{i<j}^{n} x_i x_j s_{0i} s_{ij} , \\ \cdots\cdots\cdots\cdots\cdots \\ R_k(x,\ell) = \sum_{j_1<j_2<\ldots<j_k}^{n} x_{j_1} x_{j_2} \ldots x_{j_k} s_{0j_1} s_{j_1 j_2} \ldots s_{j_{k-1} j_k} , \\ \cdots\cdots\cdots\cdots\cdots \\ R_n(x,\ell) = \sum_{j_1<j_2<\ldots<j_n}^{n} x_{j_1} x_{j_2} \ldots x_{j_n} s_{0j_1} \ldots s_{j_{n-1} j_n} = x_1 x_2 \ldots x_n s_{01} s_{12} \ldots s_{n-1,n} \end{cases} \qquad (11)$$

where $j = 1, 2, \ldots n$.

Formulae (8) and (11) enable NP focussing to be calculated for any system with known parameters. However, the reverse interests us: to find the parameters of a system comprising n lenses in terms of the degree of focussing required in the momentum range $p_{min} \div p_{max}$. As $F_n(p)$ is proportional to the multinomial of the nth power from p, then, according to the Viète theorem, the coefficients at corresponding powers of the multinomial are expressed via the roots of this multinomial as follows:

$$\begin{cases} R_1(x,\ell) = \sum_{i=1}^{n} p_i = Q_1(p_j), \\ R_2(x,\ell) = \sum_{i<j}^{n} p_i p_j = Q_2(p_j), \\ \cdots\cdots\cdots\cdots\cdots \\ R_n(x,\ell) = \sum_{i<j<\ldots<k}^{n} p_i p_j \ldots p_k = p_1 p_2 \ldots p_n = Q_n(p_j). \end{cases} \qquad (12)$$

This system of equations (12) is essential for the study of focussing systems with differing numbers of lenses.

We shall note some of the properties of this system:

a) from (11) it can be seen that R_j (x, ℓ) are symmetrical with reference to the substitution

$$\begin{cases} x_k \longrightarrow \ell_{n+k-1}, \\ \ell_k \longrightarrow x_{n+1-k}, \end{cases} \tag{13}$$

$k = 1,2 \ldots n$. Consequently, it is possible to switch from one set of unknowns to the other when solving system (12).

b) If the root $p_n \to 0$, then the nth equation of the system takes the form:

$$x_1 x_2 \ldots x_n \ell_1 \ell_2 \ldots \ell_{n-1} \ell_n = 0, \tag{14}$$

and, consequently, one of the parameters, for example ℓ_n, equals zero. By substituting $\ell_n = 0$ into all the other equations of system (12) and by changing the notation $x_n + x_{n-1} \longrightarrow x_{n-1}$, we obtain the same type of system for an (n-1)-lens system. This means that all the expressions valid for an n-lens system change at their limiting value when $p_n \to 0$ to corresponding expressions for a system containing one lens less.

c) The equations in (12) impose n conditions on 2n parameters $\{x_j, \ell_j\}$, $j = 1,2,\ldots n$. In principle, any n values from this set may be taken as unknown and the remainder made to vary like parameters. The system's solution substantially depends on which parameters are taken as unknown. In cases where all $\{x_j\}$ or $\{\ell_j\}$ are taken as unknown, the resolvent's power equals n! and solutions for $n \geqslant 3$ are not expressed in radicals.

However, it is possible to select n unknowns in such a

way that the system's resolvent will in any case be linear. In fact, system (12) is linear in relation to the following combinations of n values x_i, ℓ_j, $i > i_o$, $j > j_o$:

$$\begin{cases} y_1 = \sum\limits_{i_1 > i_o}^{n} x_i , \\ y_2 = \sum\limits_{i_1 \geqslant j_1 > j_o}^{n} \ell_{j_1} x_{i_1} , \\ \cdots\cdots\cdots\cdots\cdots\cdots\cdots \\ y_{k+1} = \sum\limits_{i_{k/2} \geqslant j_{k/2} > \ldots > i_2 \geqslant j_2 > i_1 > i_o}^{n} x_{i_1} (\ell_{j_2} x_{i_2}) \ldots (\ell_{j_{k/2}} x_{i_{k/2}}) , \\ \cdots\cdots\cdots\cdots\cdots\cdots\cdots \\ y_k = \sum\limits^{n} (\ell_{j_1} x_{i_1}) (\ell_{j_2} x_{i_2}) \ldots (\ell_{j_{k/2}} x_{i_{k/2}}) , \\ \qquad i_{k/2} \geqslant j_{k/2} > \ldots > i_2 \geqslant j_2 > i_1 \geqslant j_1 > j_o \\ \cdots\cdots\cdots\cdots\cdots\cdots\cdots \end{cases} \tag{15}$$

$$\text{here } i_o = \begin{cases} n/2, \text{ if } n \text{ is even} \\ \dfrac{n-1}{2} \text{ if } n \text{ is odd,} \end{cases}$$

$$j_o = \begin{cases} n/2 \text{ if } n \text{ is even} \\ \dfrac{n+1}{2} \text{ if } n \text{ is odd} \end{cases}$$

With these designations, the equations of (12) take the form

$$\sum_{k=i}^{n} a_{ik} y_k = b_i , \qquad i = 1, 2, \ldots, n . \tag{16}$$

The coefficients a_{ik} and the free terms b_i, which are functions of the remaining parameters, can be obtained from the equations of system (12) in each specific case.

System (15) is easily solved and all the unknowns are unambiguously expressed in terms of y_j.

2. Two-, three- and four-lens systems

A) Two-lens system.

In this case, according to (15), we obtain:

$$\begin{cases} y_1 = x_2, \\ y_2 = \ell_2 x_2. \end{cases} \tag{17}$$

System (16) then takes the form:

$$\begin{cases} y_1 + y_2 = p_1 + p_2 - x_1, \\ x_1 y_2 = p_1 p_2. \end{cases} \tag{18}$$

From (17) and (18) we find that

$$\begin{cases} \ell_2 = \dfrac{p_1 p_2}{-x_1^2 + x_1(p_1 + p_2) - p_1 p_2}, \\ x_2 = \dfrac{-x_1^2 + x_1(p_1 + p_2) - p_1 p_2}{x_1}. \end{cases}$$

The graphs illustrating the behaviour of $\ell_2(x_1)$ and $x_2(x_1)$ are shown in fig. 5. A typical feature is that, as ℓ_2 is positive, the limitation $p_2 < x_1 < p_1$ is imposed on the parameter x_1.

At the point $x_1 = \dfrac{p_1 + p_2}{2}$ the function $\ell_2(x_1)$, is at a minimum.

$$\ell_{2\,min} = \frac{4 p_1 p_2}{(p_1 - p_2)^2}. \tag{19}$$

From expression (19) it can be seen that in two-lens systems of finite length, the focussing function F(p) cannot have multiple roots.

If the length of the two-lens system is restricted by the L value, then it follows from (19) that the ratio of the roots p_2/p_1 does not exceed the value

$$\left(\frac{p_2}{p_1}\right)_{\text{макс}} = 1 + \frac{2}{L}\left(1 - \sqrt{1 + L}\right).$$

B) Three-lens system.

In this case

$$\begin{cases} y_1 = x_2 + x_3, \\ y_2 = \ell_3 x_3, \\ y_3 = \ell_3 x_2 x_3. \end{cases} \tag{20}$$

y_1, y_2, y_3 satisfy the system of equations:

$$\begin{cases} (1 + \ell_2)\, y_1 + y_2 = Q_1 - x_1, \\ \ell_2 x_1 y_1 + x_1 y_2 + (1 + \ell_2)\, y_3 = Q_2, \\ \ell_2 x_1 y_3 = Q_3. \end{cases} \tag{21}$$

From this we find

$$\begin{cases} y_1 = \dfrac{1}{\ell_2 x_1^2}\left[-x_1^3\ell_2 + x_1^2\ell_2 Q_1 - x_1\ell_2 Q_2 + (1+\ell_2) Q_3 \right] = \dfrac{a}{\ell_2 x_1^2}, \\ y_2 = \dfrac{1}{\ell_2 x_1^2}\left[x_1^3\ell_2^2 - x_1^2\ell_2 Q_1 + x_1\ell_2(1+\ell_2) Q_2 - (1+\ell_2)^2 Q_3 \right] = \dfrac{b}{\ell_2 x_1^2}, \\ y_3 = \dfrac{Q_3}{\ell_2 x_1}. \end{cases}$$

By solving system (20) with reference to x_2, x_3 and ℓ_3, we obtain:

$$\begin{cases} x_2 = y_3 / y_2 = Q_3 x_1 / b, \\ x_3 = y_1 - x_2 = \dfrac{ab - x_1^3 \ell_2 Q_3}{b \ell_2 x_1^2}, \\ \ell_3 = y_2 / x_3 = \dfrac{b^2}{ab - x_1^3 \ell_2 Q_3}. \end{cases} \qquad (22)$$

From the condition that the distance between the lenses is positive ($\ell_3 > 0$), it follows that

$$ab - x_1^3 {}_2 Q_3 > 0. \qquad (23)$$

Figure 6 shows the area within which condition (23) is met when $p_1 = 1$, $p_2 = 0{,}35$ and $p_3 = 0{,}2$. The formulae in (22) offer a complete solution to the problem of finding parameters which will describe three-lens systems in terms of a given focussing function (F(p). Fig. 7a shows the path of beams in one of the systems, as calculated from these formulae when the focussing function (Fig. 7b) has the roots $p_1 = 1$, $p_2 = 0{,}35$ and $p_3 = 0{,}2$.

C) Four-lens system.

For a four-lens system y_j, $j = 1,2,3,4$ take the form:

$$\begin{cases} y_1 = x_3 + x_4 , \\ y_2 = \ell_3 x_3 + \ell_3 x_4 + \ell_4 x_4 , \\ y_3 = \ell_4 x_3 x_4 , \\ y_4 = \ell_3 \ell_4 x_3 x_4 . \end{cases} \tag{24}$$

They comply with the linear system:

$$\begin{cases} (1 + \ell_2) y_1 + y_2 = Q_1 - x_1 - (1 + \ell_2) x_2 , \\ \ell_2 x_1 y_1 + [(1 + \ell_2) x_2 + x_1] y_2 + (1 + \ell_2) y_3 + y_4 = Q_2 - \ell_2 x_1 x_2 , \\ \ell_2 x_1 x_2 y_2 + \ell_2 x_1 y_3 + [(1 + \ell_2) x_2 + x_1] y_4 = Q_3 , \\ \ell_2 x_1 x_2 y_4 = Q_4 . \end{cases} \tag{25}$$

By solving system (24) with reference to x_3, x_4, ℓ_3 and ℓ_4, **we obtain:**

$$\begin{aligned} \ell_3 &= y_4 / y_3 , \\ \ell_4 &= (y_2 y_3 - y_1 y_4)^2 / (y_1 y_2 y_3 - y_1^2 y_4 - y_3^2) y_1 , \\ x_3 &= y_3^2 / (y_2 y_3 - y_1 y_4) , \\ x_4 &= (y_1 y_2 y_3 - y_1^2 y_4 - y_3^2) / (y_2 y_3 - y_1 y_4) . \end{aligned} \tag{26}$$

We shall not write out the explicit expressions for y_1, y_2, y_3 and y_4 **obtained from the solution of linear system (25) as they are too cumbersome. The requirement** $\ell_3 > 0$, $\ell_4 > 0$ **leads to two conditions imposed on the free parameters** x_1, x_2 **and** ℓ_2:

$$\begin{cases} y_3 > 0, \\ y_1 y_2 y_3 - y_1^2 y_4 - y_3^2 > 0. \end{cases} \tag{27}$$

Fig. 8 shows the focussing function and beam path for one of the four-lens systems, as calculated from the formulae in (26).

A similar analysis can be made of systems comprising a larger number of lenses.

3. Some properties of the systems examined

The above formulae were used as a basis for the study of the behaviour of solutions as functions of parameters which remained free. Figures 9 and 10 illustrate the most characteristic dependences for three- and four-lens systems. At the limits of the areas defined by conditions (23) and (27), the overall lengths of the systems $S_n = \sum_{j=1}^{n} \ell_j$ become infinite. Within these areas (viz. fig. 9b, 10b), the S_n function has a minimum value. This value is determined by the position of the roots of the focussing function. The behaviour of $S_{n\,min}(p_1, p_2, \ldots p_n)$ was studied for $n \leqslant 4$. When any of the roots p_k tends towards p_{k+1}, the $S_{n\,min}$ function increases smoothly and so

$$\lim_{p_k \to p_{k+1}} S_{n\,min}(p_1, \ldots p_k, p_{k+1}, \ldots p_n) = \infty . \qquad (28)$$

This behaviour of the $S_{n\,min}$ function means that, after specific limitations have been placed on the system's geometry, we cannot select roots at random in $F_n(p)$ and also cannot expect to find multiple roots. This condition in turn restricts the focussing quality in these systems.

Figures 11 and 12 show graphs of the behaviour of $S_{3\,min}(1, p_2, 1/5)$ and $S_{4\,min}(1, 2/5, 1/5, p_4)$ respectively. The curves in these diagrams behave according to (28).

We note one other consequence arising from (28). Let the roots $p_1 > p_2 > \ldots > p_{n-1} > p_n > 0$. If, at fixed values of $p_1, p_2, \ldots p_{n-1}$, the root $p_n \to 0$, then $S_{n\,min}$ decreases smoothly, and, as follows from property (b) of system (12), $S_{n\,min} \to S_{n-1\,min}$.

Hence, the following inequality is valid

$$S_{n\ min}(p'_1,\ldots p'_{n-1},\ p_n) > S_{n-1\ min}(p'_1,\ldots p'_{n-1}). \qquad (29)$$

Therefore, by increasing the number of lenses and thus improving focussing due to the appearance of new roots in $F_n(p)$, the length of the S_n system is increased. Thus, an optimization of the system's length and focussing power is tied up with an optimization of the number of lenses in the system. In order to obtain a characteristic of the degree of particle focussing, we shall examine the values of $F_n(p)$ at the extreme points p_1^{ex} and p_2^{ex}, where $p_{k+1} < p_k^{ex} < p_k$, $k = 1,2$. We denote

$$\left| F_n\ (p_i^{ex}) \right| = B_i\ (p_1,\ p_2,\ \ldots p_n).$$

Fig. 13 includes a set of graphs illustrating the behaviour of $S_{3\ min}\ (1,\ p'_2,\ p_3)$, $B_1\ (1,\ p'_2,\ p_3)$ and $B_2\ (1,\ p'_2,\ p_3)$ for cases where $p'_2 = 0{,}25 - 0{,}5$. If we confine ourselves to systems for which $S_{3\ min} < 20$, it can be seen from these graphs that, in the range $0{,}3 < p_2 < 0{,}4$, systems can be obtained in which $F_3\ (p)$ $\sim 15 - 20\%$ throughout the momentum range $p_3 \div p_1$.

Fig. 14 includes a similar set of graphs for a four-lens system where $p'_1 = 1$, $p'_2 = 0{,}35$, $p'_3 = 0{,}3 - 0{,}1$ and $p_4 < p'_3$. The limit points at $p_4 \longrightarrow 0$ correspond to the three-lens systems. It is clear that the introduction of another lens improves focussing somewhat, but also substantially increases the length of the system.

4. Objectives consisting of thin lenses

There are a number of reasons why it may be necessary to swap some of the strong lenses in the systems examined above for equivalent objectives consisting of a set of weak lenses. Let us examine the matrix of a symmetrical objective comprising three lenses, i.e. an objective with two outer lenses of the same focussing strength equidistant from a centre lens with a focussing strength of k_2.

$$\begin{pmatrix}1 & 0\\ -k_1 & 1\end{pmatrix}\begin{pmatrix}1 & \ell\\ 0 & 1\end{pmatrix}\begin{pmatrix}1 & 0\\ -k_2 & 1\end{pmatrix}\begin{pmatrix}1 & \ell\\ 0 & 1\end{pmatrix}\begin{pmatrix}1 & 0\\ -k_1 & 1\end{pmatrix} =$$

$$= \begin{pmatrix}1 & \ell\\ -k_1 & 1-k_1\ell\end{pmatrix}\begin{pmatrix}1 & 0\\ -k_2 & 1\end{pmatrix}\begin{pmatrix}1-k_1\ell & \ell\\ -k_1 & 1\end{pmatrix} \qquad (30)$$

Here

$$k_i = \frac{x_i}{p} = \text{const} \cdot b_i . \qquad (31)$$

It is easy to show that the following relations occur:

$$\begin{pmatrix}1 & \ell\\ -k_1 & 1-k_1\ell\end{pmatrix} = \begin{pmatrix}1 & \ell/(1-k_1\ell)\\ 0 & 1\end{pmatrix}\begin{pmatrix}1/(1-k_1\ell) & 0\\ -k_1 & 1-k_1\ell\end{pmatrix},$$

$$\begin{pmatrix}1-k_1\ell & \ell\\ -k_1 & 1\end{pmatrix} = \begin{pmatrix}1-k_1\ell & 0\\ -k_1 & 1/(1-k_1\ell)\end{pmatrix}\begin{pmatrix}1 & \ell/(1-k_1\ell)\\ 0 & 1\end{pmatrix}.$$

By using these, we obtain from (30)

$$\begin{pmatrix}1 & \ell/(1-k_1\ell)\\ 0 & 1\end{pmatrix}\begin{pmatrix}1 & 0\\ -k & 1\end{pmatrix}\begin{pmatrix}1 & \ell/(1-k_1\ell)\\ 0 & 1\end{pmatrix}, \qquad (32)$$

where

$$k = (1-k_1\ell)\,[\,2k_1 + k_2(1-k_1\ell)\,]. \qquad (33)$$

Hence, it is clear that except for the terms $k_1\ell \ll 1$, this objective is **similar to one lens with a focussing strength k, located in the centre of the objective. In order to switch from one lens to an equivalent objective comprising two lenses, it is sufficient to pose** $k_2 = 0$ **in** (33). **In this case**

$$k_1 = \frac{1}{\ell}\,(1-\sqrt{1-k\ell}). \qquad (34)$$

Fig. 15-1 shows the focussing difference $\Delta F_{12} = F_1 - F_2$ in one of the three-lens systems and in the equivalent system consisting of two-lens objectives. The difference in focussing amounts to a few per cent. only in a narrow area of low momenta, and for the rest of the range $\Delta F_{12} \sim 1\%$.

It is interesting to study a case where all the lenses in the objective are the same. For a three-lens objective with equidistant lenses, the lens strength is then determined from the equation

$$k_1^3 - \frac{4}{\ell} k_1^2 + \frac{3}{\ell^2} k_1 - \frac{k}{\ell^2} = 0, \qquad (35)$$

whose physical solution is the value:

$$k_1 = \frac{2}{3\ell} \left[2 - \sqrt{7} \cos 1/3 \cdot (\pi - \varphi) \right], \qquad (36)$$

where φ = arc cos $\dfrac{20 + 27k\ell}{14\sqrt{7}}$

Fig. 15-2 shows the difference $\Delta F_{13} = F_1 - F_3$ for a system comprising objectives of this type. The difference is $\sim 2\%$ throughout practically the entire momentum range.

5. Effect of an extended target

All the calculations have so far been made on the assumption that the NP are produced at a point source s situated at a distance ℓ_1 from the first lens in the focussing system. However, in practice the length of the target must be taken into account.

Let us assume that the particle was produced at a point situated at a distance ℓ from the first lens. The matrix $T(\ell)$, which describes the motion of this particle in the focussing system, equals:

$$T(\ell) = \begin{bmatrix} T_{11} & T_{21} \\ T_{12} & T_{22} \end{bmatrix} \begin{bmatrix} 1 & \ell - \ell_1 \\ 0 & 1 \end{bmatrix} = \begin{bmatrix} T_{11} & T_{11}(\ell - \ell_1) + T_{21} \\ T_{12} & T_{12}(\ell - \ell_1) + T_{22} \end{bmatrix} \qquad (37)$$

Particle focussing is determined by the element $T_{22}(\ell)$:

$$F_n(p,\ell) = T_{12}(p)(\ell-\ell_1) + T_{22}(p). \qquad (38)$$

The element T_{12} is proportional to the multinomial of the n - 1 power in terms of p. At points p_j where $T_{12}(p_j) = 0$, focussing does not depend on the position of the production point ℓ.

Fig. 16 shows the curves for particle focussing in one of the three-lens systems when $\Delta\ell = \ell - \ell_1 = -0{,}45$, 0, 0,45, and 0,6 (in units of ℓ_1). It can be seen that the focussing quality for different target points varies only slightly.

III. Focussing system consisting of parabolic lenses

As a practical example, we shall examine a device consisting of linear-focussing units, that is of parabolic lenses. The investigation will be performed with reference to the conditions at the IHEP proton synchrotron. The focussing properties of this system indicate that an intense neutrino flux can be obtained throughout the energy range available at this accelerator. Our selection of a particular system was based on the requirement that the focussed NP beam should be obtained within a distance of no more than 15-20 m., that is ~ 10% of the overall decay length. It was also desirable that the lateral deviation of the beam at the output from the system should not exceed the size of the neutrino detector.

As is well-known, one half of the neutrinos obtained from meson decay remain within the emission angle $\Theta = \frac{m_o c^2}{E}$, where m_o is the meson's rest mass and E its energy. The main part of the neutrino spectrum up to E_ν = 10 GeV consists of neutrinos from the decay of π-mesons of $E_\pi \leqslant$ 25 GeV, for which $\Theta \geqslant 1/200$. For K-mesons of 60 GeV $\Theta \geqslant 1/120$. Therefore, NP should only be focussed up to angles of 5-10 mrad.

One of the main characteristics of a focussing system is its acceptance. By equipping systems with wide-aperture units, it is possible to capture the particle flux in a large angular range. However, in practice the lens apertures are restricted by specific values. The length of a parabolic lens is a square-law function of its radius and, using the system of units selected, equals

$$z = \frac{500}{3} \frac{p_o x r^2}{I . \ell_1} ,$$

where I is the current in ka, r is the radius in cm., ℓ_1 is the distance scale in m., p_o is the scaling momentum in GeV/c and x is the lens strength, a dimensionless value. (If the parabolic lenses are made from aluminium, pulsed currents of up to 700-900 ka can be passed through the lens, due to the strength properties of this material). By widening the aperture, the length and number of lenses in the objectives can be increased. The angular and momentum distribution of the mesons was taken into account when setting the aperture.

Fig. 17 includes curves which indicate the dependence on momentum of an angle which contains a given percentage of mesons*. The lens radii were selected so that 80-90% NP capture was ensured in the given momentum range.

The focussing system selected includes three lenses ensuring a high percentage of capture and good NP focussing in the range 5-50 GeV/c with comparatively small apertures. The scaling factors used are ℓ = 1,15 m and p_o = 15 GeV/c. The first and third lenses are 1 - 1,5 m long. For reasons of manufacture and power supply, it is advisable to change these lenses for objectives consisting of shorter lenses of equivalent effect (formulae 30, 36). Therefore, the first and third lenses are replaced by three-lens and two-lens objectives respectively (table 1b). By using objectives instead of single lenses, particle absorption in the lens material is not considerably increased. In fact, the actual path of a particle in the lens wall is mainly determined by the factor

* The curves were calculated by V.N. Folomeshkin.

$$\frac{dz}{dr} = 2br \ , \tag{39}$$

and particles traversing the lens at large radii have a bigger path in it than those which pass close to the axis. When the strong lens is divided up into weaker lenses, as can be seen from expressions (31) and (33), the following relationship occurs correct to within $K_1 \ell \ll 1$:

$$b = \Sigma b_i . \tag{40}$$

Therefore, the overall length of a particle's path in the lens material remains virtually the same.

The main characteristics of the system are given in table 1(A).

Table 1

I = 800 ka $\qquad\qquad$ p_o = 15 GeV/c

	Lens no.	x	ℓ (M)	η (CM)	z (CM)
A	1	0.490	1.15	10.0	132.0
	2	0.126	2.87	13.0	58.0
	3	0.057	8.52	25.0	96.0
B	1	0.186	0.69	8.0	32.0
	2	0.186	0.46	10.0	50.5
	3	0.186	0.57	10.5	55.5
	4	0.126	2.30	13.0	58.0
	5	0.029	8.13	25.0	49.0
	6	0.029	0.57	25.0	49.0

A. Parameters of the optimal three-lens system

B. Parameters of the system after the switch from lenses to objectives.

In order to reduce the dependence of particle absorption on the radius of traversal through the lens, the thickness of the lens walls may be varied and made thinner as the radius increases.

We studied the effect of an extended target on the focussing and acceptance of the system, the characteristics of which are given in table 1(B). The quality of focussing of the whole NP beam at various target lengths remains virtually the same. The curves in Fig. 16, corresponding to this system at p_o = 15 GeV/c and l_1 = 1.15 m, illustrate this fact. Fig. 18 shows the dependence of the angle of capture on momentum at various positions of the meson production point. It can be seen that the system's acceptance only changes significantly in the region 5-10 GeV/c. A system with this level of acceptance ensures that a large percentage of the mesons produced on an extended target are captured (Fig. 19).

The properties of the focussing system were studied in a thin-lens approximation. In order to check the accuracy of the results, we wrote a program to compute particle trajectories for a given surface profile according to formulae (P.4) and (P.5). The respective focussing curves are shown in Fig. 20 and it can be seen that they coincide satisfactorily. The difference between the results from the "thin" and "thick" approximations for this system does not exceed 5%. There is virtually no focussing dependence on the particle's angle of entrance into the system.

One of the peculiarities of a parabolic lens is the neck linking the vertices of the paraboloids. The field has no effect on the particles within the diameter of the neck. Using the optimal system as an example, the effect of a neck 3 cm in diameter leads to a considerable angular dependence when focussing NP emitted from the target in an angular cone of less than 15-20 mrad. Typical curves are shown in Fig. 21. We should point out that the presence of the neck has a relatively strong effect on the lenses of the first objective.

In order to allow for geometric aberrations, the trajectory should be calculated from the more precise formulae (P.1) and (P.2).

IV. Calculation of neutrino spectra

1. Program

Fig. 22 is a block diagram of the device used for producing the neutrino beam. Primary protons of 76 GeV energy are extracted from the accelerator and focussed on a target several millimetres in diameter. Secondary charged particles (π- and K-mesons) escape from the target, pass through the focussing system, decay and form fluxes of μ-mesons, neutrinos and antoneutrinos:

$$\begin{aligned} \pi^+ &\to \mu^+ \nu \\ K^+ &\to \mu^+ \nu \\ \pi^- &\to \mu^- \tilde{\nu} \\ K^- &\to \mu^- \tilde{\nu} \end{aligned} \qquad (41)$$

The neutrino flux is cleared of any μ-meson impurity by iron shielding ($\frac{dE}{dz} = -1{,}35$ GeV/cm) located at the end of the decay channel.

The probability of the production of secondary particles in the range $x \div x + \Delta x$ equals:

$$\omega_1 = \frac{\Delta x}{\lambda_1} \exp\left(-\frac{x}{\lambda_1}\right), \qquad (42)$$

where λ_1 is the length of the nuclear interaction. For aluminium and beryllium $\lambda_1 = 41$ cm. and for copper $\lambda_1 = 16.7$ cm. The probability of the absorption of a meson produced at point x equals:

$$\omega_2 = \exp\left(-\frac{L - x}{\lambda_2}\right) \qquad (43)$$

for escape through the target's end face and

$$\omega_2 = \exp\left(-\frac{r}{\Theta\, \lambda_2}\right) \qquad (44)$$

for escape through the target's lateral face.

In formulae (43) and (44) L is the target length, r is the target radius and $\lambda_2 \approx 2\lambda_1$ is the length of the meson interaction.

Scattering in the target material is disregarded in the calculations.

In order to describe the angular and momentum distribution of the secondary particles, we use the Ranft formula /7/:

$$\frac{\partial^2 N}{\partial p\, \partial \Omega} = A_1 p^{A_2} p_o^{A_3} \exp\left(-B_1 p^{B_2} p_o^{-B_3} - C_1 p^{C_2} p_o^{C_3} \Theta^{C_4}\right), \qquad (45)$$

where p (GeV/c) is the secondary particle's momentum, p_o(GeV/c) the primary proton's momentum and Θ (rad) the secondary particle's production angle.

Table II shows the values of parameters A_1, A_2 ... C_4 in relation (45) for various particles.

The differential spectra $\frac{\partial^2 N}{\partial p \partial \Omega}$ of the π^+-and K^+ mesons, calculated from this formula are shown in figures 23 and 24.

Table II

A_1	A_2	A_3	B_1	B_2	B_3	C_1	C_2	C_3	C_4
0,036	0,86	1,08	2,93	1,81	-1,47	3,31	1,18	0,20	1,38
$1{,}744.10^{-3}$	0,9627	1,1369	2,9195	1,7914	-1,5238	3,3291	1,3251	0,1046	1,4725
0,021	0,71	1,24	3,13	1,65	-1,29	2,99	1,20	0,22	1,42
$6{,}078.10^{-3}$	0,7865	1,2994	3,1509	1,1696	-1,2712	2,9912	1,2617	0,1500	1,4357

The probability of the escape of a meson with a momentum within the range $p \div p + \Delta p$ and within the angular aperture $\Theta \div \Theta + \Delta\Theta$ equals

$$\omega_M = \frac{\partial^2 N}{\partial p\, \partial \Omega}\, 2\pi \sin\Theta\, \Delta p\, \Delta\Theta. \qquad (46)$$

Mesons which have escaped from the target decay with the probability

$$\omega_3 = \frac{\Delta z}{\lambda_3} \exp\left(-\frac{z}{\lambda_3}\right), \qquad (47)$$

where z is the distance from the production point to the decay point (m) and λ_3 is the decay length of the meson (m). For π-mesons, $\lambda_3 = 55p$ (GeV/c) and for K mesons $\lambda_3 = 7p$ (GeV/c). The momentum of a neutrino produced from the decay of a meson equals

$$p_\nu = \frac{2\gamma p^*_\nu}{(1 + \gamma^2 \mathrm{tg}^2 \alpha_\nu)}, \qquad (48)$$

where $\gamma = \frac{E}{mc^2}$, E is the meson's energy, m is the meson's mass, α_ν is the neutrino's escape angle and p^*_ν is the neutrino's energy in the meson's rest frame.

For π-meson decay $p^*_\nu = 0{,}0298$ GeV/c and for K meson decay $p^*_\nu = 0{,}2356$ GeV/c.

Neutrino momenta are distributed uniformly in the range from 0 to $2\gamma p^*_\nu$ and therefore the probability of the production of a neutrino with a momentum of p_ν equals $\frac{1}{2\gamma p^*_\nu}$.

Due to the finite dimensions of the detector, only a part of the neutrino hits it. The hit probability (viz. Fig.25) equals:

$$\omega_4 = \begin{cases} 0, & \text{if } |s - R| < R_0 \\ 1, & \text{if } s + R < R_0 \\ \frac{1}{\pi} \arccos \frac{R^2 + s^2 - R_0^2}{2sR} & \text{in other cases.} \end{cases} \qquad (49)$$

The energy spectrum of the neutrino flux passing through the detector is calculated by integration in terms of the target length, decay path, escape angles and momenta of the mesons; the form

of the decay $K \to \mu\nu$, equalling 63.5%, is also taken into account.

$$\frac{dN}{dp_\nu} = 2\pi \int_{p_{min}}^{p_{max}} dp \int_0^{\Theta_{max}} d\Theta \int_0^L dx \int_0^D dz \; \frac{\omega_1 \omega_2 \omega_3 \omega_4 \sin\Theta}{2\gamma p^* \lambda_1 \lambda_3} \cdot \frac{\partial^2 N}{\partial p \partial \Omega}, \quad (50)$$

$$p_{min} = \frac{m p_\nu}{2p^*} \left[1 + \left(\frac{p_\nu^*}{p_\nu} \right)^2 \right]. \quad (51)$$

Two programs were written for this purpose:

a) a program to calculate the paths of secondary charged particles inside and outside the focussing device.

b) a program to calculate integral (50) and using program (a) as a sub-program.

The first program determines the co-ordinates of the points of entry of the particles into the units of the focussing system and, using the solution of the motion equations for a particle in a magnetic field (P.4 and P.5), it calculates the point co-ordinates and emission angles by the iteration method. The program can work out the trajectories for focussing systems whatever the arrangement of their units' inner surfaces.

The main program calculates the quadruple integral (50) by the "imbedded integrals" method. Each imbedded integral is considered to be an integrand function and the outer integral relating to it is calculated as a single integral. Each single integral is found by the trapezoid method with a fixed integration step. When integrating in terms of meson momenta, it is essential to take into account the strong dependence of the neutrino's emission angle on p in the p value range close to p_{min}. Therefore, the integration step Δp is selected so that the variation of the angle α_ν does not exceed a certain value $\Delta\alpha_\nu$. The value $\Delta\alpha_\nu$ is fixed so that the detector is not 'missed' during integration. The integration step in terms of the mesons' emission angles $\Delta\Theta$ is selected in the same way. Variations in the protons' flight distance in the target (ℓ) and in the mesons'

flight distance to the decay point (z) are determined from the conditions:

$$\Delta l \ll \lambda_1$$
$$\Delta z \ll \lambda_3 .$$

The lay-out of the main program is shown in Fig.26. The values of the integration steps and limits used in the calculations are given below. The accuracy with which the neutrino spectrum is calculated under these conditions is ~10%.

Table III

p_{max} U	$\Delta\alpha_\nu$	$(\Delta p)_o$	Θ_{min} Θ_{max}	$\Delta\Theta$	Δl	Δz
(p + 20) GeV/c	0,002 rad.	0.5 GeV/c	0,0 0,1 rad.	0,002	5 cm(Cu)	15m.

2. Neutrino spectra

For the given focussing system (table 1B) a study was made of the dependence of the neutrino spectrum on the decay length R_{decay} and the detector's radius R_∂. The meson shielding was 60 m. thick and the radius of the decay tunnel was 1.25 m. The detector was placed 10 m. from the shielding.

When the target-detector distance is increased, the probability of meson decay also increases but the probability of neutrinos hitting the detector drops. The variation in the spectrum according to the path length is shown in Fig. 27. For a detector with R_∂ = 0.5 m, the best spectrum is obtained at a target-detector distance of ~ 200 m. Fig. 28 shows the absolute value of this spectrum. For comparison, it also shows the spectra for ideal focussing and for NP focussing using the horn + reflector system /5/. The neck of the parabolic lenses has no substantial effect on the neutrino spectrum.

Figs. 29 and 30 show the neutrino spectra for a detector of 1 m. diameter. An increase in the detector's radius produces on average a 3-fold increase in neutrino intensity. Under these conditions, the real spectrum differs from the ideal spectrum by a factor of 1,5. For the given detector, the total length of 200 m. is also one of the best.

The authors are extremely grateful to S.S. Gershtejn, G.I. Sil'vestrov, L.L. Danilov, E.P. Kuznetsov, A.I. Mukhin, V.N. Folomeshkin and A.M. Frolov for many useful discussions, and also to A.A. Logunov, R.M. Sulyaev, A.A. Naumov and V.I. Kotov for their unfailing interest and support.

Bibliography

1. S. van der Meer. CERN, 61-7.

2. E.B. Forsyth, L.M. Lederman, J. Sunderland. CERN, 65-32.

3. R.B. Palmer. Symposium on Neutrino Physics, CERN, 1965.

4. A. Asner, Ch. Iselin. CERN, 65-17.

5. G.C. Sacerdotti, E. Fiorini et al. *High Energy Neutrino Beams for the Serpukhov Accelerator.* Milano. 1969.

6. V.L. Auslender, V.N. Bajer et al. Proceedings of the IV International Accelerators Conference, P.282, M. 1964.

   L.L. Danilov, S.N. Rodionov, G.I. Sil'vestrov. Zhurnal' Tekhnicheskoj Fiziki, 37, 914, 1967.

7. T. Ranft. "An empirical formula for the Spectra". MPS/Int, MV/EP, 66-4;
   T. Ranft. "An empirical formula for the Spectra". MPS/Int, MV/EP, 66-7.

The document was received by the publishing group on
19 October 1970.

V. Appendix

The magnetic field set up by current I in an axisymmetric system equals $H = \frac{\mu_0 I}{2\pi r}$, where $\mu_0 = 4\pi \cdot 10^{-7}$ (we shall use the MKSA system).

The motion equations for mesons in this field take the form:

$$\begin{cases} \dfrac{d^2 r}{dt^2} - r\left(\dfrac{d\phi}{dt}\right)^2 = -\dfrac{k}{r}\dfrac{dz}{dt}, \\ \dfrac{d^2 z}{dt^2} = k\dfrac{1}{r}\dfrac{dr}{dt}, \\ \dfrac{d}{dt}\left(r^2\dfrac{d\phi}{dt}\right) = 0, \\ k\left(\dfrac{м}{сек}\right) = \dfrac{ec^2\mu_0 I}{2\pi E} = 1{,}8\cdot 10^4 \dfrac{I\,(ка)}{E\,(Гэв)} \end{cases}$$

By integrating the last two equations, we obtain:

$$\dot{z} = \dot{z}_0 + k\ell n\frac{r}{r_0}, \qquad r^2\dot{\phi} = r_0^2\dot{\phi}_0 = \text{const},$$

r_0, z_0 and ϕ_0 are the particles' initial co-ordinates. By substituting these expressions into the first equation, we obtain:

$$\ddot{r} = -f(r), \qquad f(r) = -r\dot{\phi}^2 + \frac{k}{r}\left(\dot{z}_0 + k\ell n\frac{r}{r_0}\right).$$

By rewriting this equation in the form

and considering that $\dfrac{d\dot{r}^2}{dt} = -2\dot{r}f(r)$

we obtain $\int_{r_0}^{r}\frac{1}{r}\ell n\frac{r}{r_0}\,dr = \frac{1}{2}\ell n^2\frac{r}{r_0}$ и $\dot{r} = \dfrac{dr}{dz}\dot{z}$,

$$\frac{dr}{dz} = \pm\frac{\sqrt{v^2 - \dfrac{\dot{\phi}_0^2 r_0^4}{r^2} - \left(\dot{z}_0 + k\ell n\dfrac{r}{r_0}\right)^2}}{\dot{z}_0 + k\ell n\, r/r_0} \qquad (A.1)$$

Here $v^2 = \dot{r}^2 + \dot{z}^2 + r^2\dot{\phi}^2$ is the particle velocity, a motion invariant. Consequently, the mesons' trajectory in a parabolic lens is generally determined by the formula:

$$z_{вых} = z_o \pm \int_{r_o}^{r_{вых}} \frac{\left(\dot{z}_o + k \ell n \frac{r}{r_o}\right) dr}{\sqrt{v^2 - \frac{\dot{\phi}_o^2 r_o^4}{r^2} - \left(\dot{z}_o + k \ell n \frac{r}{r_o}\right)^2}}, \qquad (A.2)$$

where r_{emiss} and z_{emiss} are the particles' co-ordinates when they emerge from the lens.

The trajectory equation may be simplified somewhat by omitting the velocity's azimuthal component $v_\varphi = \frac{\dot{\phi}_o^2 r_o^4}{r^2}$ and introducing the particle's dip angle α as a variable:

$$\begin{cases} z_{вых} = z_o \pm \dfrac{r_o v \exp(-\dot{z}_o / k)}{k} \displaystyle\int_{\arcsin(\alpha_{вых} \cos \alpha_{вых})}^{\alpha_{вх}} d\alpha \cos\alpha \, e^{\frac{v \cos\alpha}{k}} \\ z_{вых} = r_o e^{\frac{v}{k}(\cos \alpha_{вых} - \cos \alpha_o)} \end{cases} \qquad (A.3)$$

If, moreover, $\frac{v}{k}$ is taken to be $\ll 1$, formula (A.1) takes the form:

$$\frac{dr}{dz} = \pm \sqrt{\alpha_{вх}^2 - \frac{2k}{\dot{z}_o} \ell n \frac{r}{r_o}}. \qquad (A.4)$$

By integrating (A.4), we obtain an explicit form for the particle trajectory in the field of the parabolic lens for a random emission angle

$$z = z_o \pm \sqrt{\frac{\pi \dot{z}_o}{2k}} r_o e^{\frac{\dot{z}_o}{2k} \alpha_{вх}^2} \left[\Phi\left(\frac{\dot{z}_o}{2k} \alpha_{вх}\right) - \Phi\left(\sqrt{\frac{\dot{z}_o}{2k}} \alpha_{вх} - \ell n \frac{r_{вых}}{r_o}\right)\right], \qquad (A.5)$$

where $\Phi(x) = \frac{2}{\sqrt{\pi}} \int_0^x e^{-\xi^2} d\xi$ -is the error function.

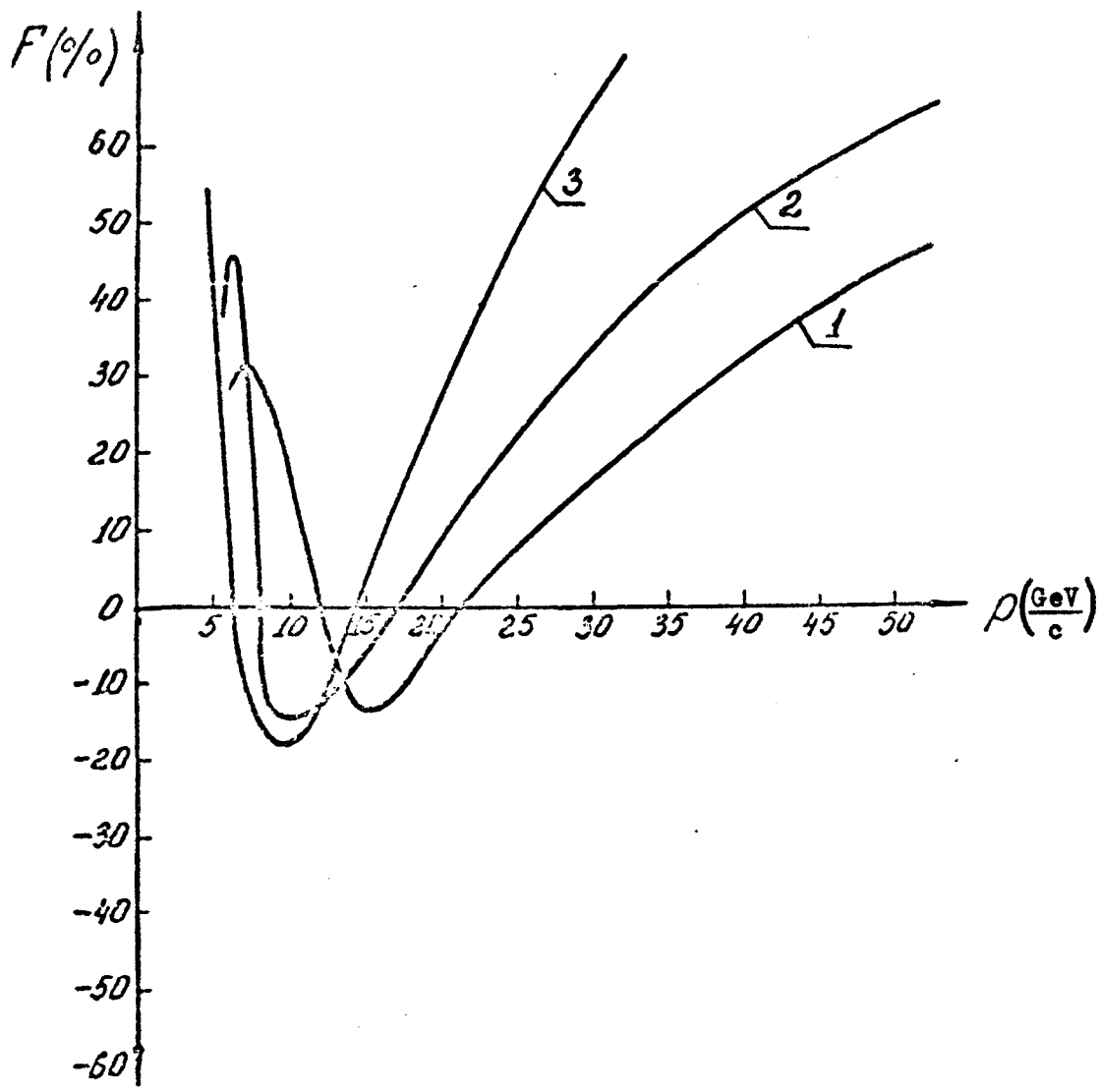

Fig. 1. Focussing curves of the horn + reflector system for different particle entrance angles into the system:
1 - $\alpha_{entr.}$ = 20 mrad; 2 - $\alpha_{entr.}$ = 30 mrad;
3 - $\alpha_{entr.}$ = 40 mrad.

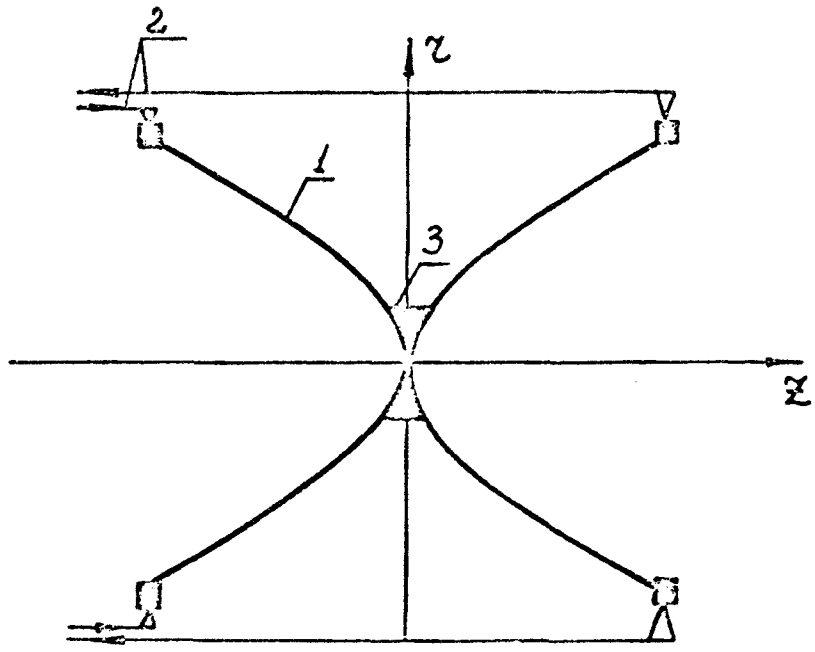

Fig. 2. Parabolic lens. 1 - paraboloid of revolution, 2 - current supply, 3 - neck.

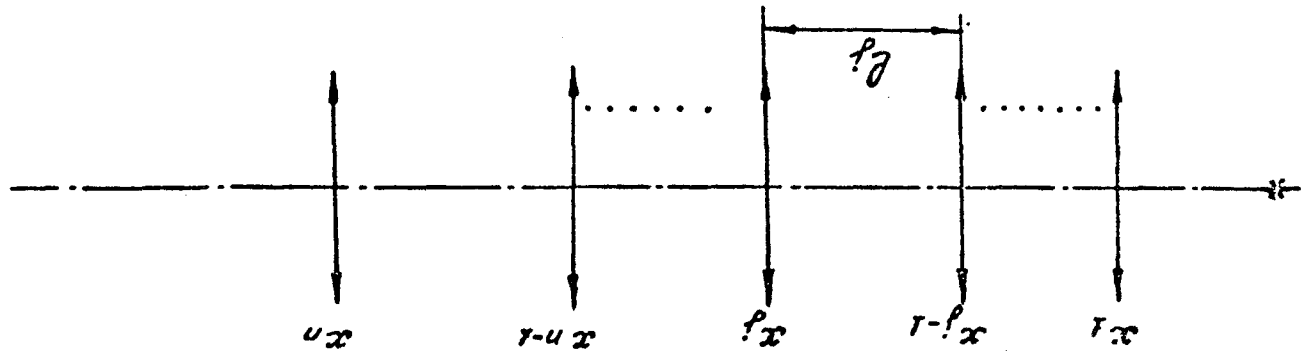

Fig. 3. System comprising n thin lenses.

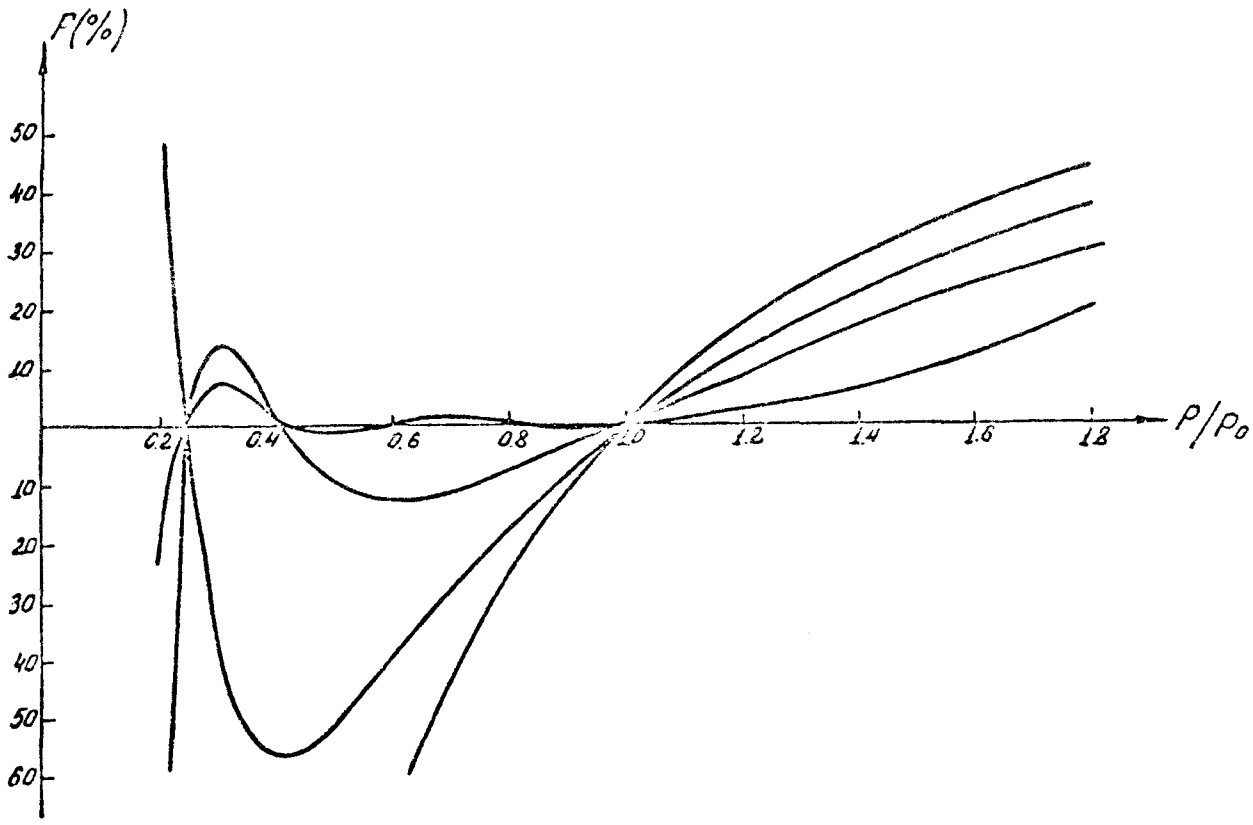

Fig. 4. Variation in focussing when the number of roots in a given momentum range is increased.

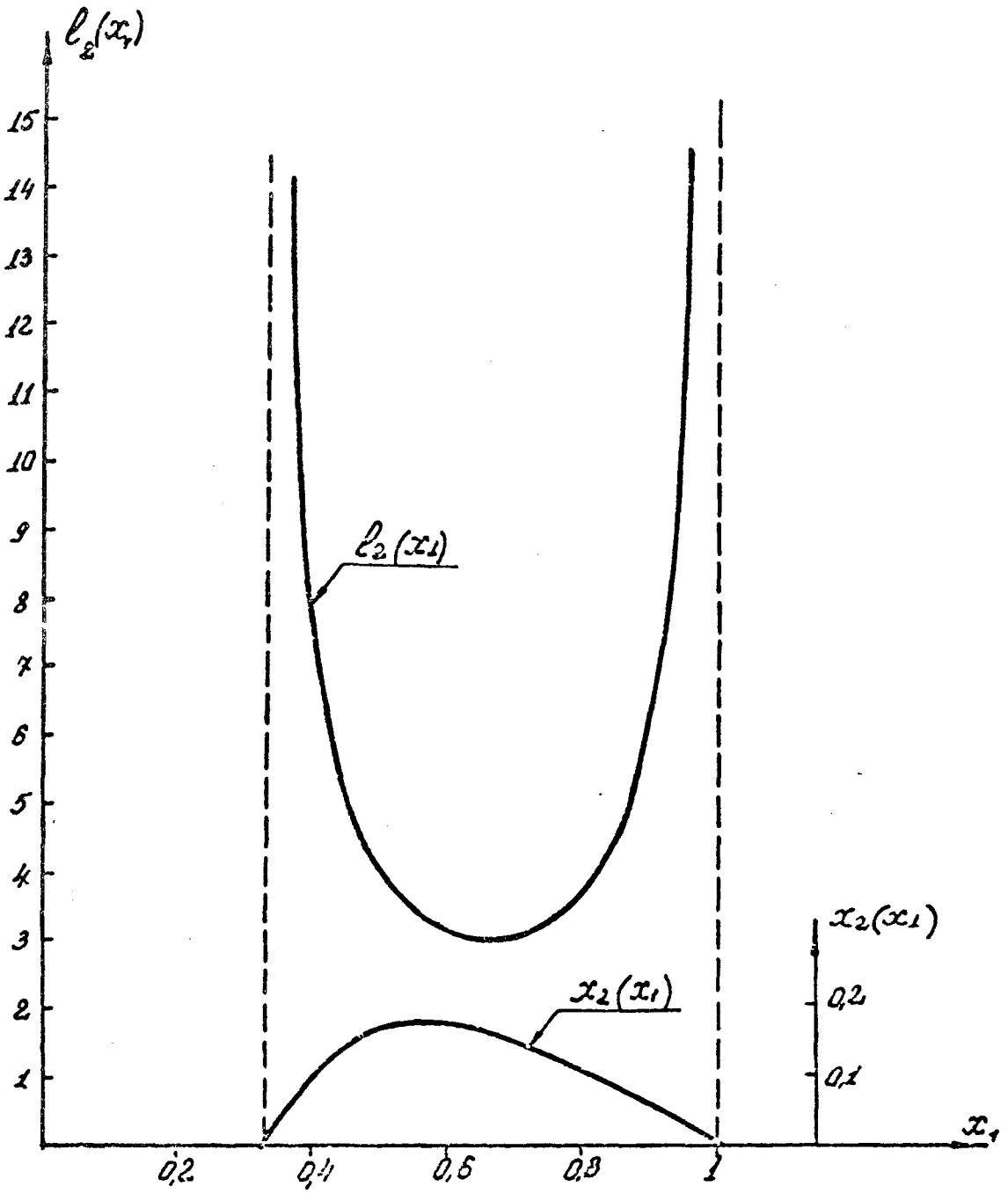

Fig. 5. Two-lens system. Behaviour of $\ell_2(x_1)$ and $x_2(x_1)$ for $p_1 = 1$, $p_2 = 1/3$.

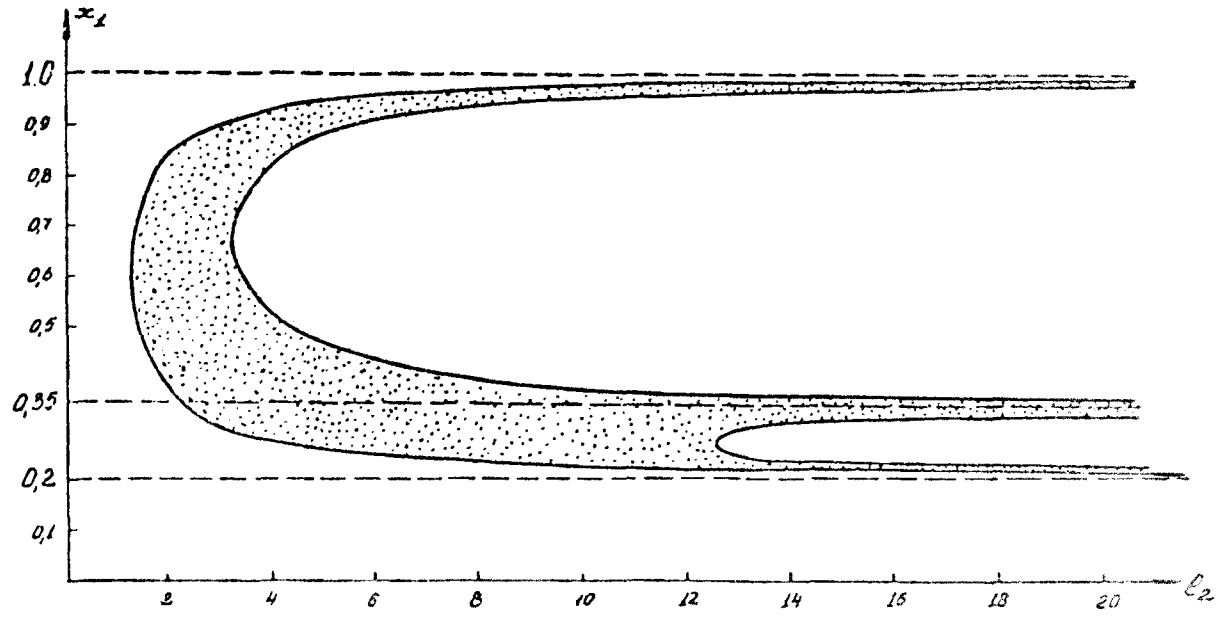

Fig. 6. Three-lens system: $p_1 = 1$; $p_2 = 0{,}35$; $p_3 = 0{,}2$.
The region within which $\ell_3(x_1, \ell_2) > 0$ is marked by dots.

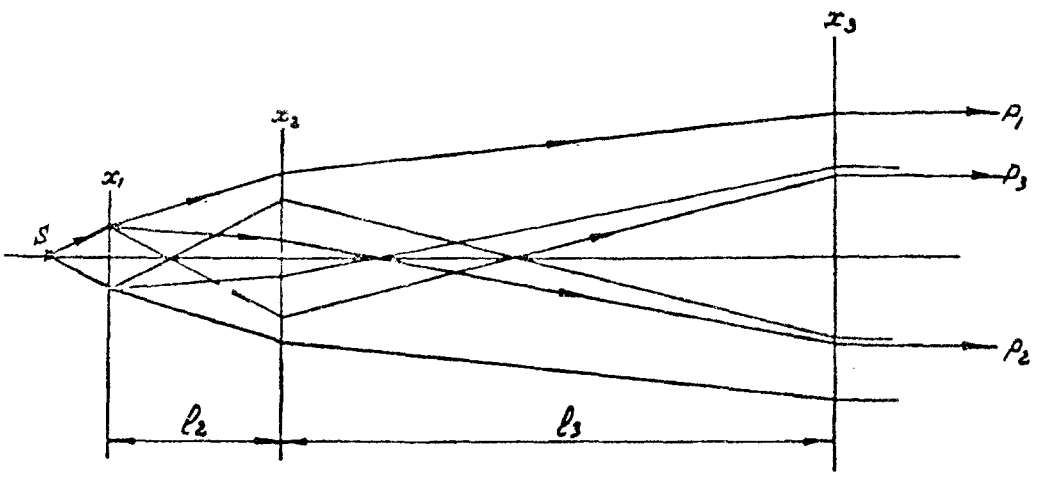

a.

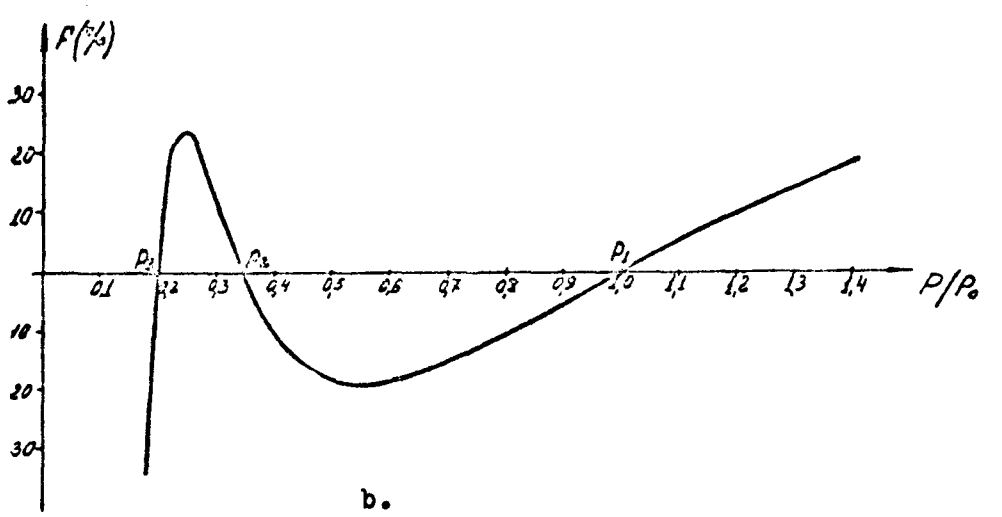

b.

Fig. 7. a) Path of beams in one of the three-lens systems. The parameters of the system are: $\ell_2 = 3{,}0$; $\ell_3 = 9{,}6$; $x_1 = 0{,}4$; $x_2 = 0{,}14$; $x_3 = 0{,}043$.

b) Focussing in this system. The following momenta emerge in parallel: $p_1 = 1$, $p_2 = 0{,}35$, $p_3 = 0{,}2$.

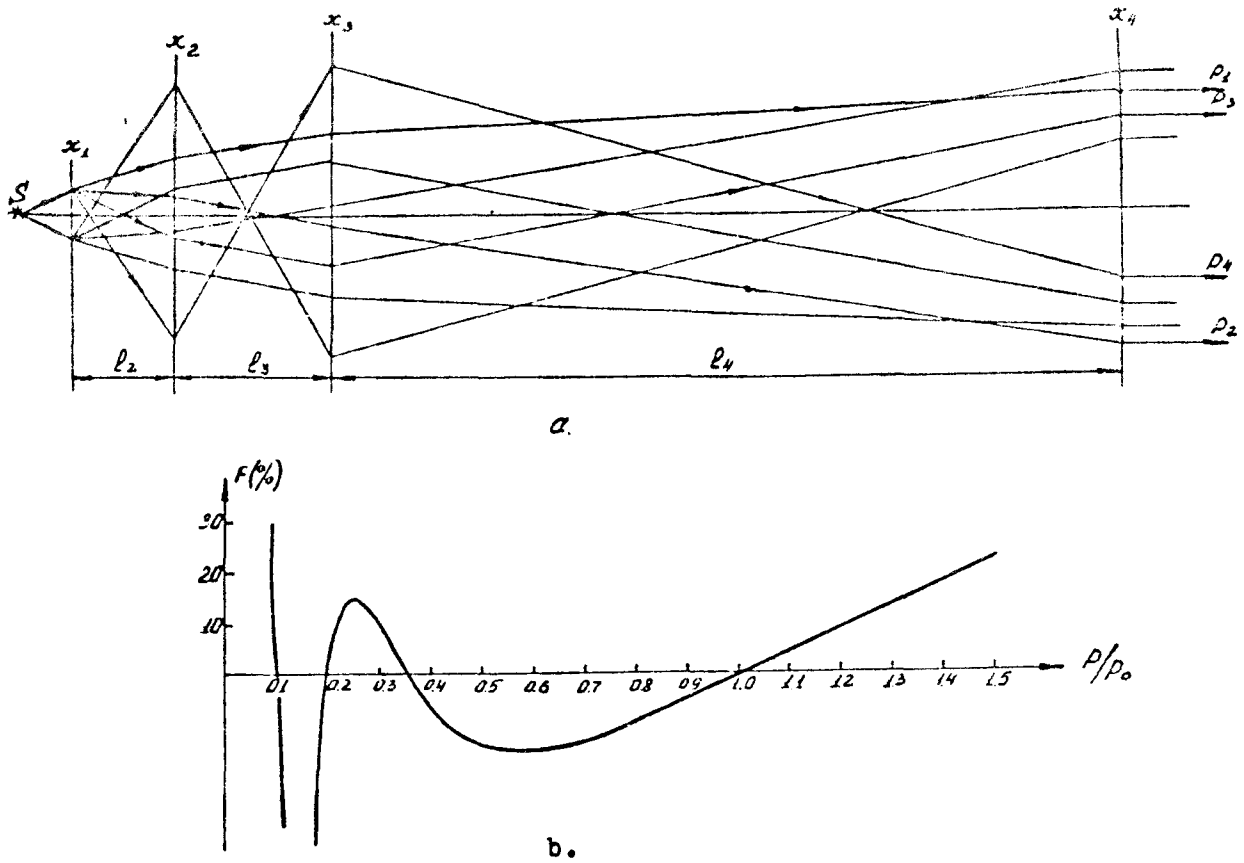

Fig. 8. a) Path of beams in one of the four-lens systems. The parameters of the system are: $l_2 = 2,0$; $l_3 = 3,1$; $l_4 = 15,4$; $x_1 = 0,40$; x_2 $0,13$; $x_3 = 0,07$; $x_4 = 0,02$.

b) Focussing in this system. The following momenta emerge in parallel: $p_1 = 1$; $p_2 = 0,35$; $p_3 = 0,2$; $p_4 = 0,1$.

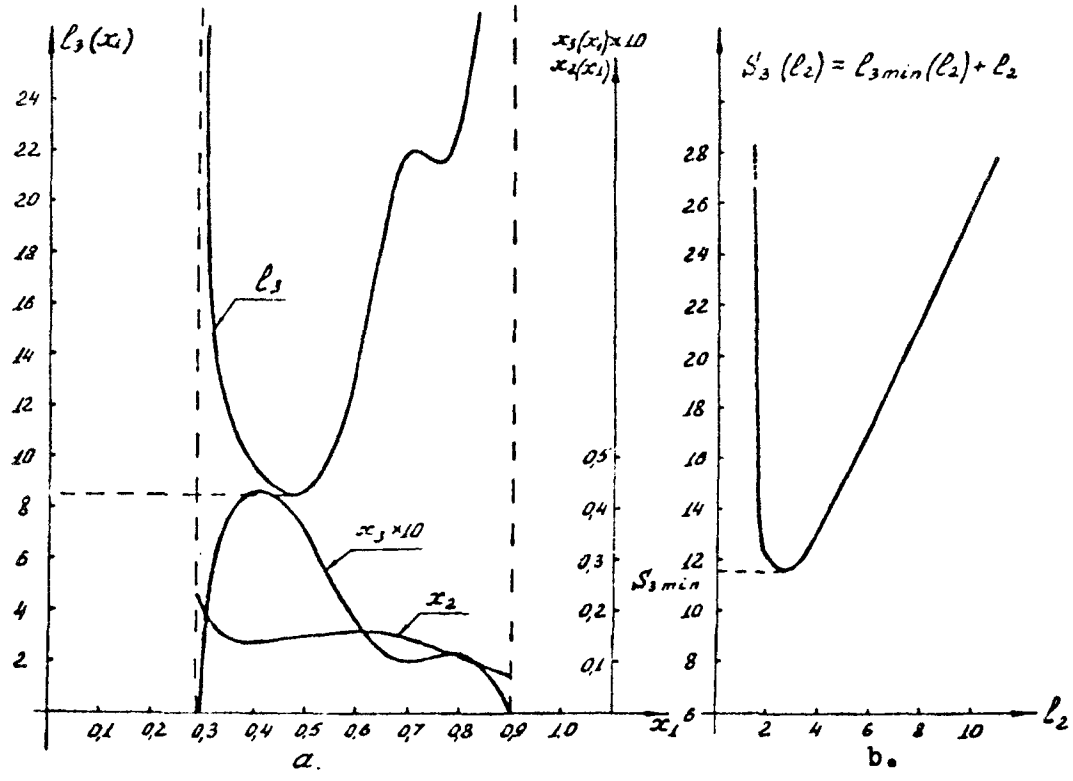

Fig. 9. Three-lens system: $p_1 = 1$; $p_2 = 0{,}35$; $p_3 = 0{,}2$.
a) Dependence of x_2, x_3, ℓ_3 on x_1 at $\ell_2 = 3$.
b) Behaviour of S_3 as a function of ℓ_2.

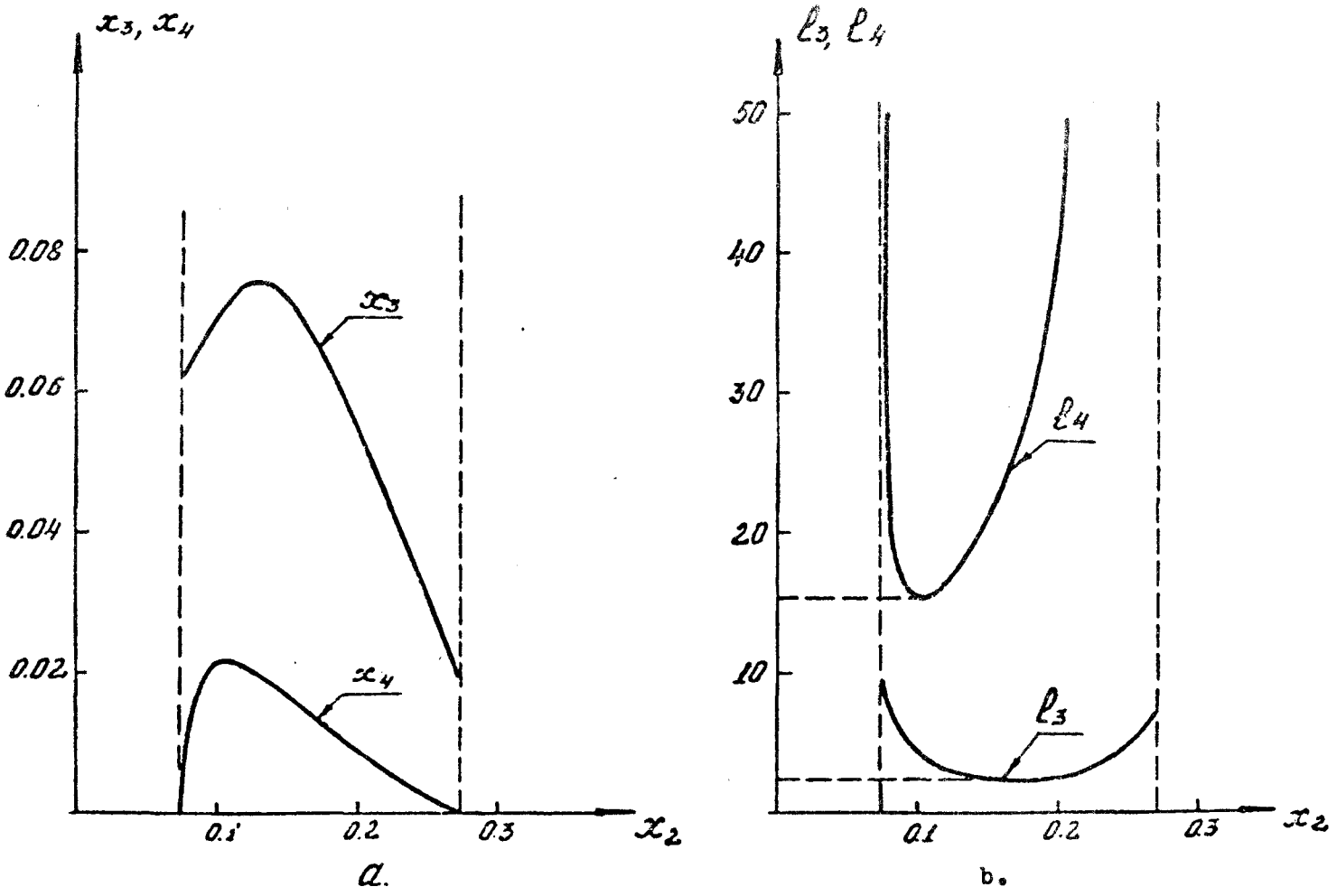

Fig. 10. Four-lens system: $p_1 = 1$; $p_2 = 0{,}35$; $p_3 = 0{,}2$; $p_4 = 0{,}1$.
Dependences:
a) of lens strength x_3, x_4 and
b) of geometry l_3, l_4 on x_2.
In the graphs $l_2 = 2{,}0$ and $x_1 = 0{,}35$.

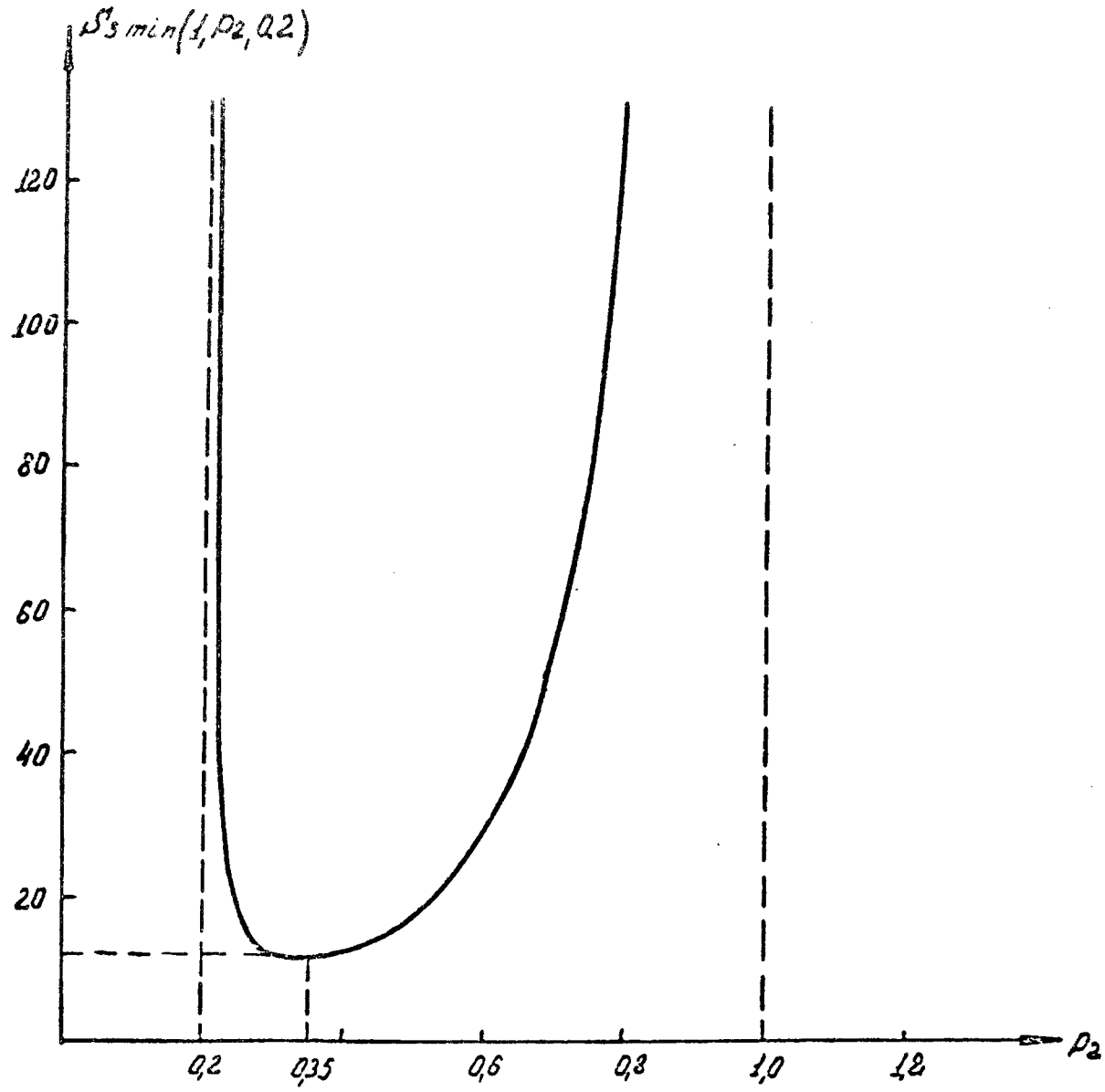

Fig. 11. Behaviour of $S_{3\ min}\ (1;\ p_2;\ 0{,}2)$. At $p_2 \longrightarrow 0{,}2$ and $p_2 \longrightarrow 1$, $S_{3\ min}\ (1;\ p_2;\ 0{,}2) \longrightarrow \infty$.

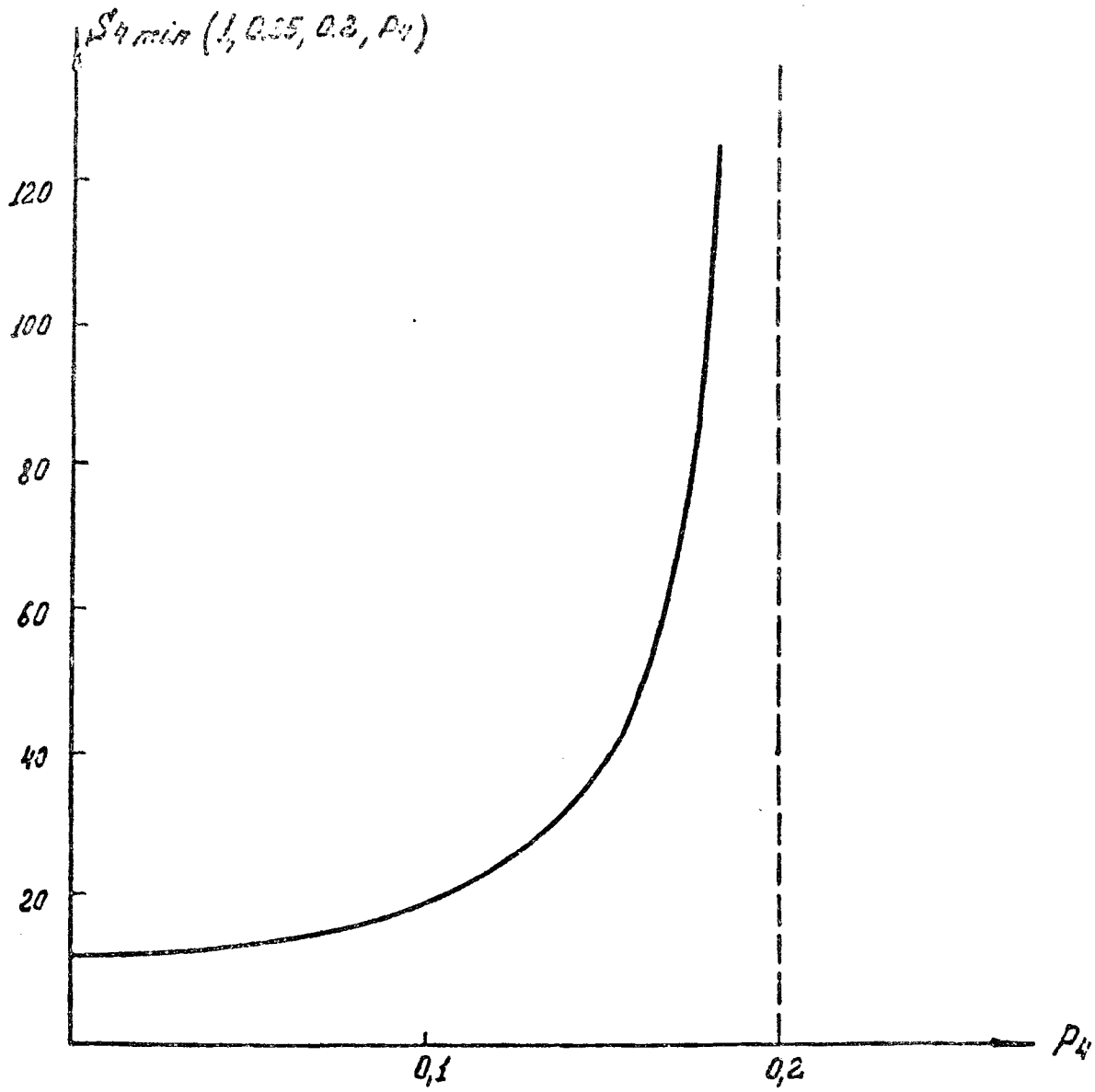

Fig. 12. Behaviour of $S_{4\ min}$ (1; 0,35; 0,2; p_4) When $p_4 \longrightarrow 0{,}2$, $S_{4\ min} \longrightarrow \infty$, when $p_4 \longrightarrow 0$, $S_{4\ min} \longrightarrow S_{3\ min}$ (1; 0,35; 0,2).

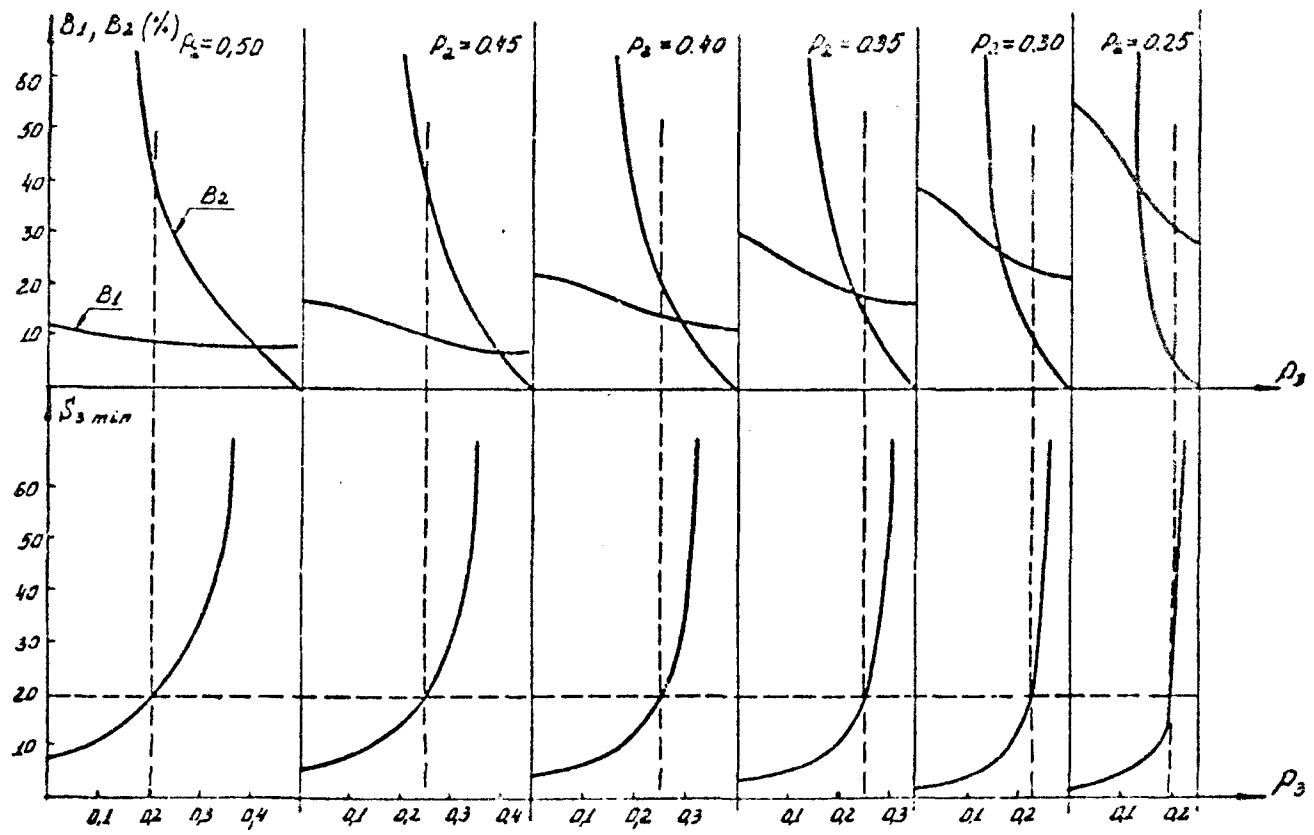

Fig. 13. Three-lens system. Set of curves $S_{3\ min}$ (1; p_2'; p_3). B_1 (1; p_2'; p_3), B_2 (1; p_2'; p_3) when p_2' = 0,5 – 0,25. The regions where $S_{3\ min} \leqslant 20$ lie to the left of the vertical hatched lines.

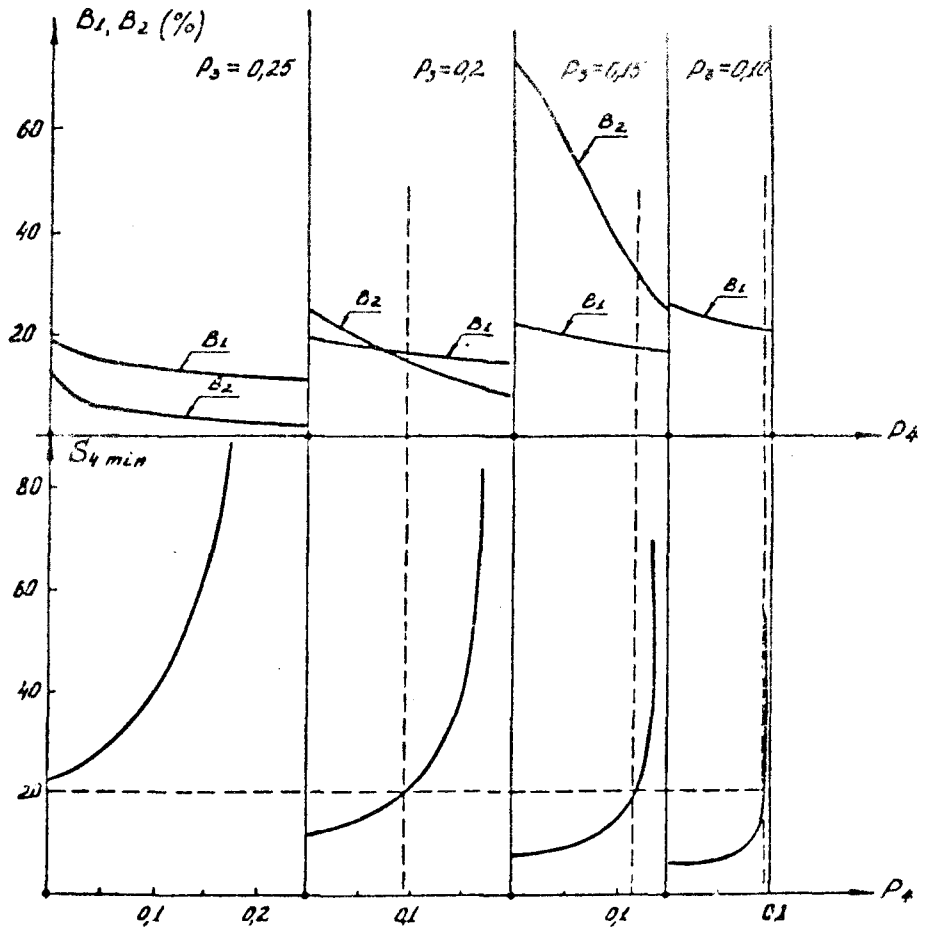

Fig. 14. Four-lens system. Set of curves $S_{4\ min}$ (1; 0,35; p_3'; p_4), B_1 (1; 0,35; p_3'; p_4), B_2 (1; 0,35; p_3'; p_4) when p_3' = 0,25 - 0,10.

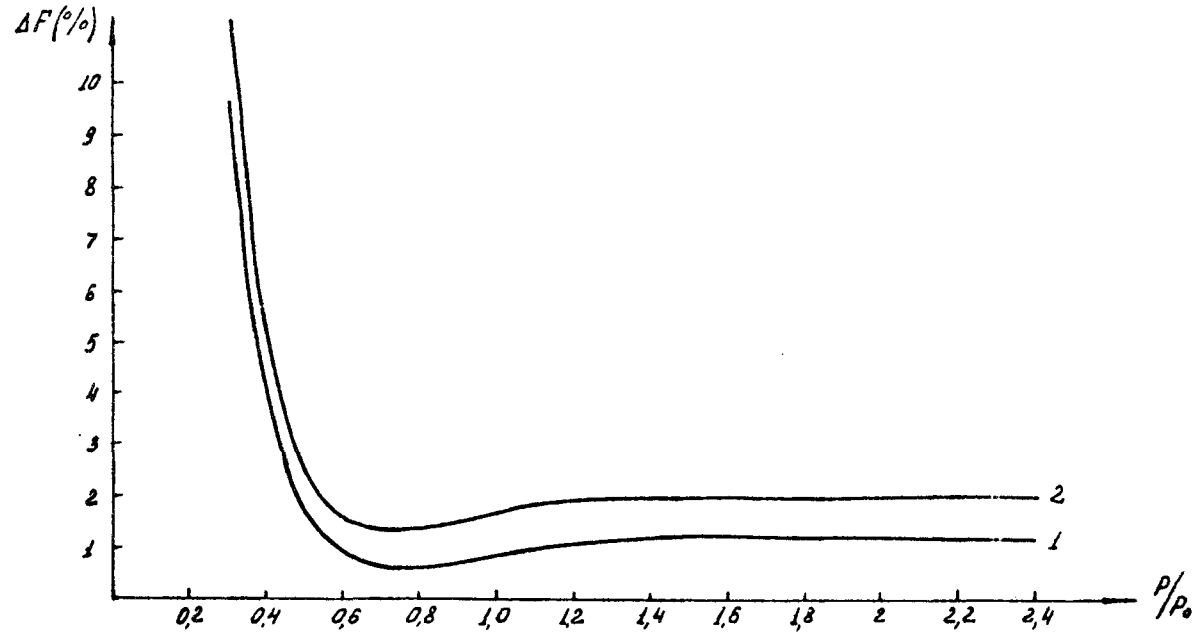

Fig. 15. Focussing variation in a system when single lenses are replaced by objectives. 1 - two-lens objectives, 2 - three-lens objectives.

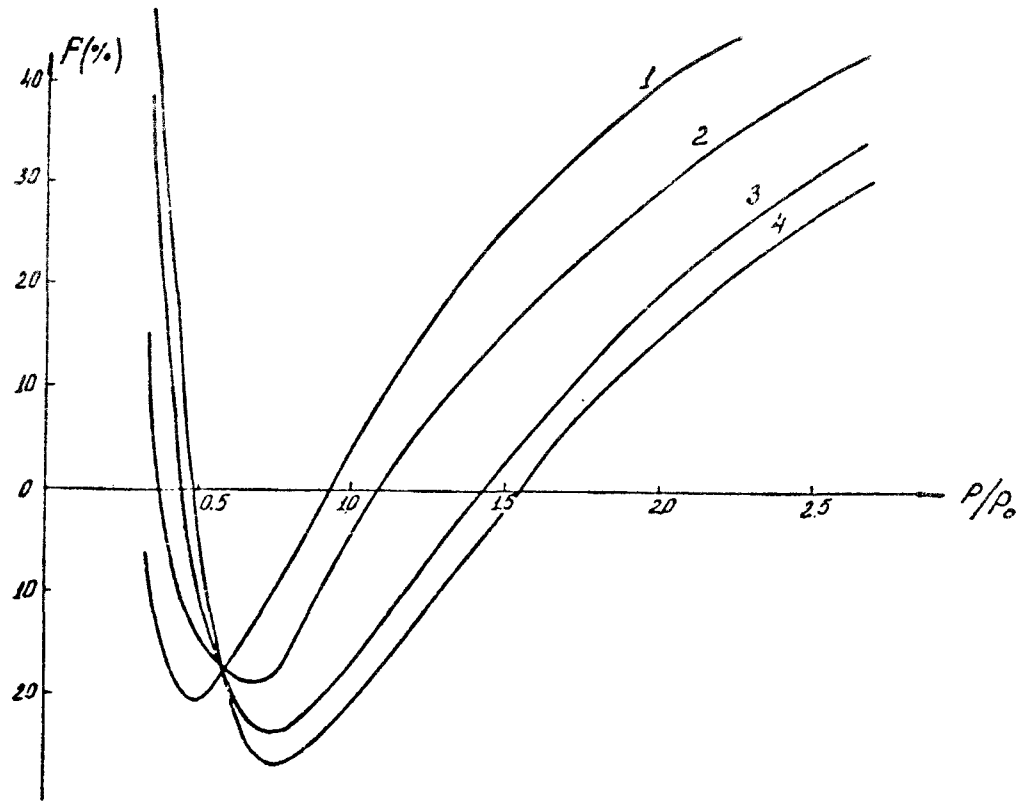

Fig. 16. Effect of an extended target on particle focussing:
1 - $\Delta\ell$ = -0,45; 2 - $\Delta\ell$ = 0; 3 - $\Delta\ell$ = 0,45; 4 - $\Delta\ell$ = 0,6.

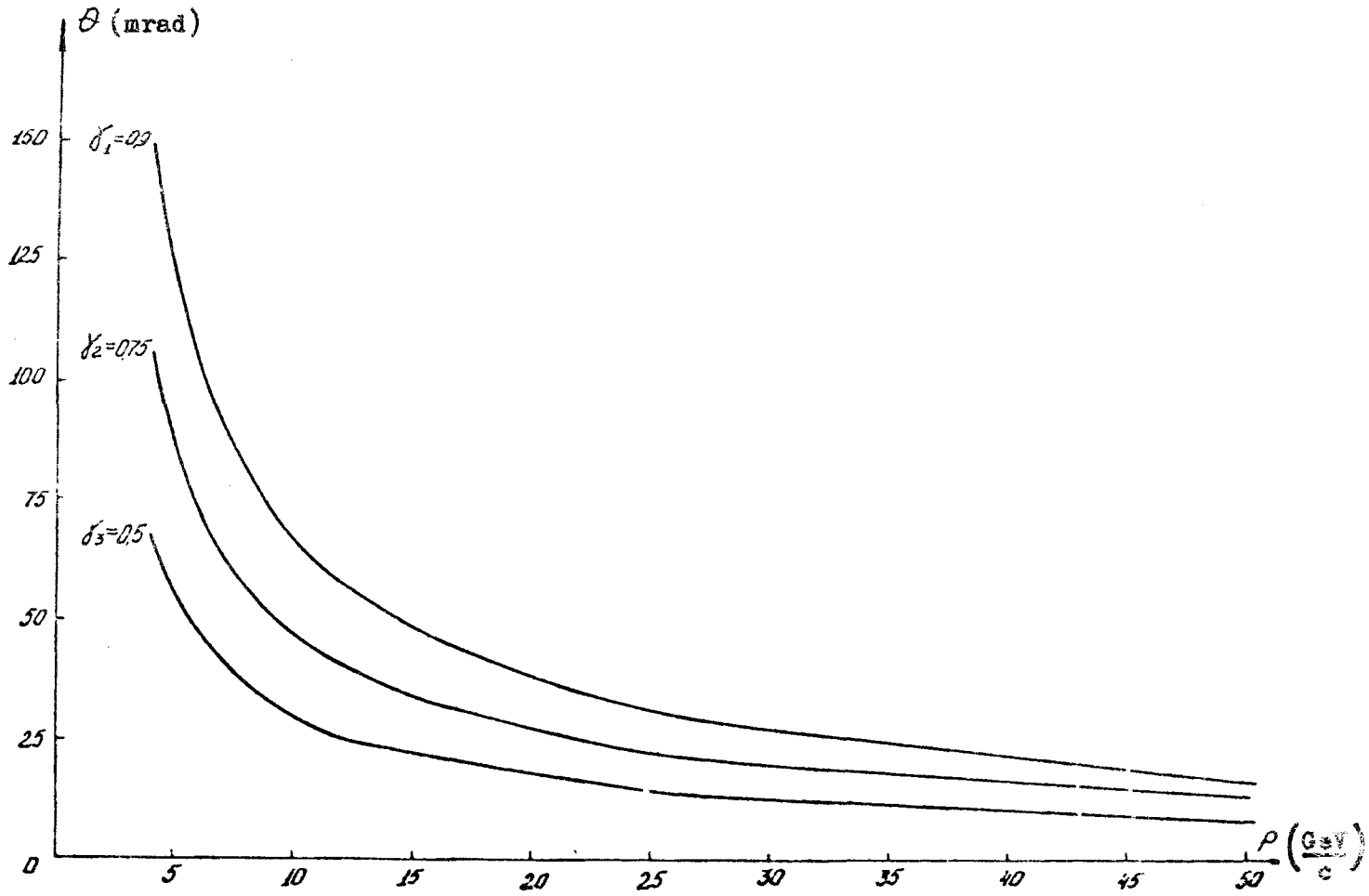

Fig. 17. Dependence of the emission angle $\Theta(\gamma)$ on momentum for π-mesons. The cases shown represent 90%, 75% and 50% particle emission.

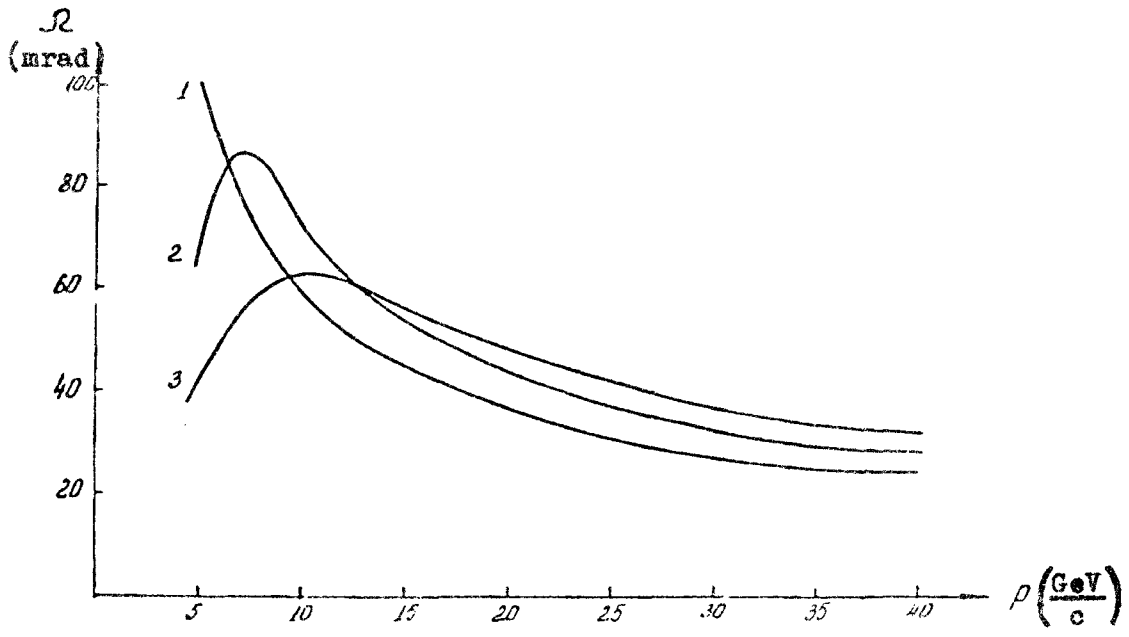

Fig. 18. Effect of an extended target on the angle of capture: 1 - $\Delta\ell$ = -50 cm; 2 - $\Delta\ell$ =0; 3 - $\Delta\ell$ = 50 cm.

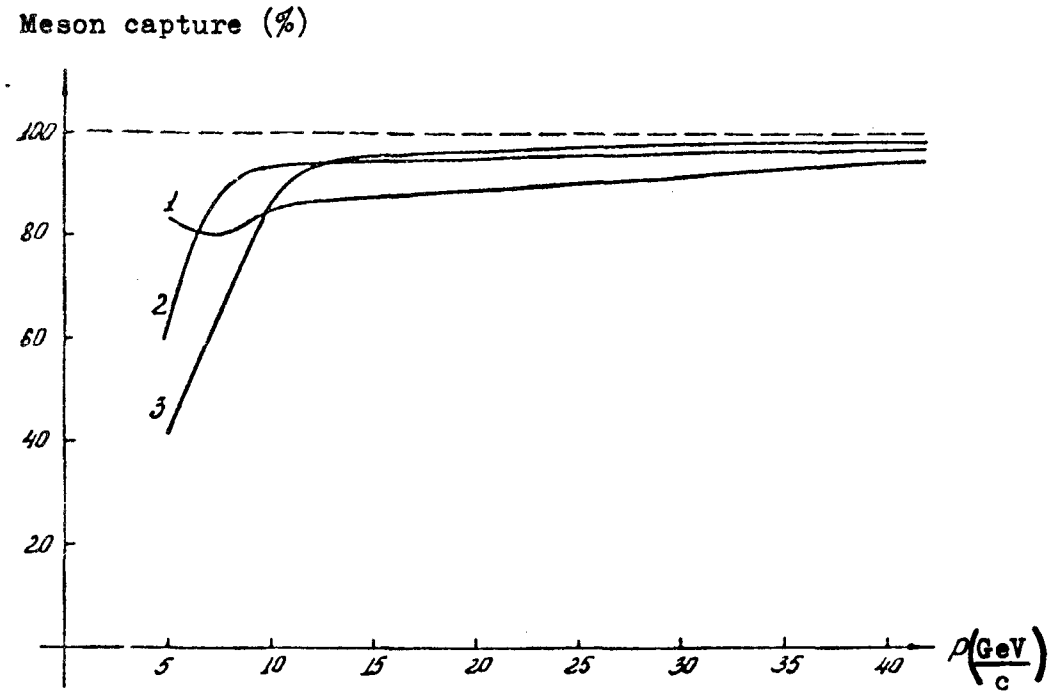

Fig. 19. Effect of an extended target on the percentage of mesons captured: 1 - $\Delta\ell$ = -50 cm; 2 - $\Delta\ell$ =0; 3 - $\Delta\ell$ = 50 cm.

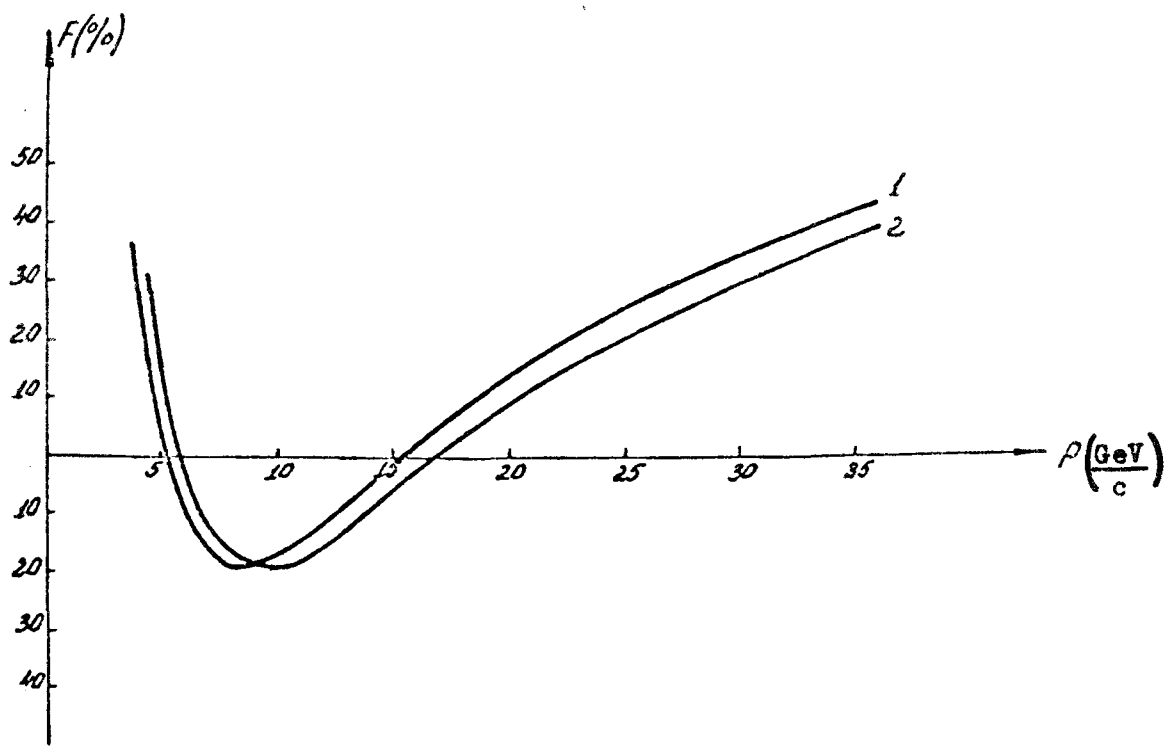

Fig. 20. Focussing curves in a: (1) thin and (2) thick lens approximation.

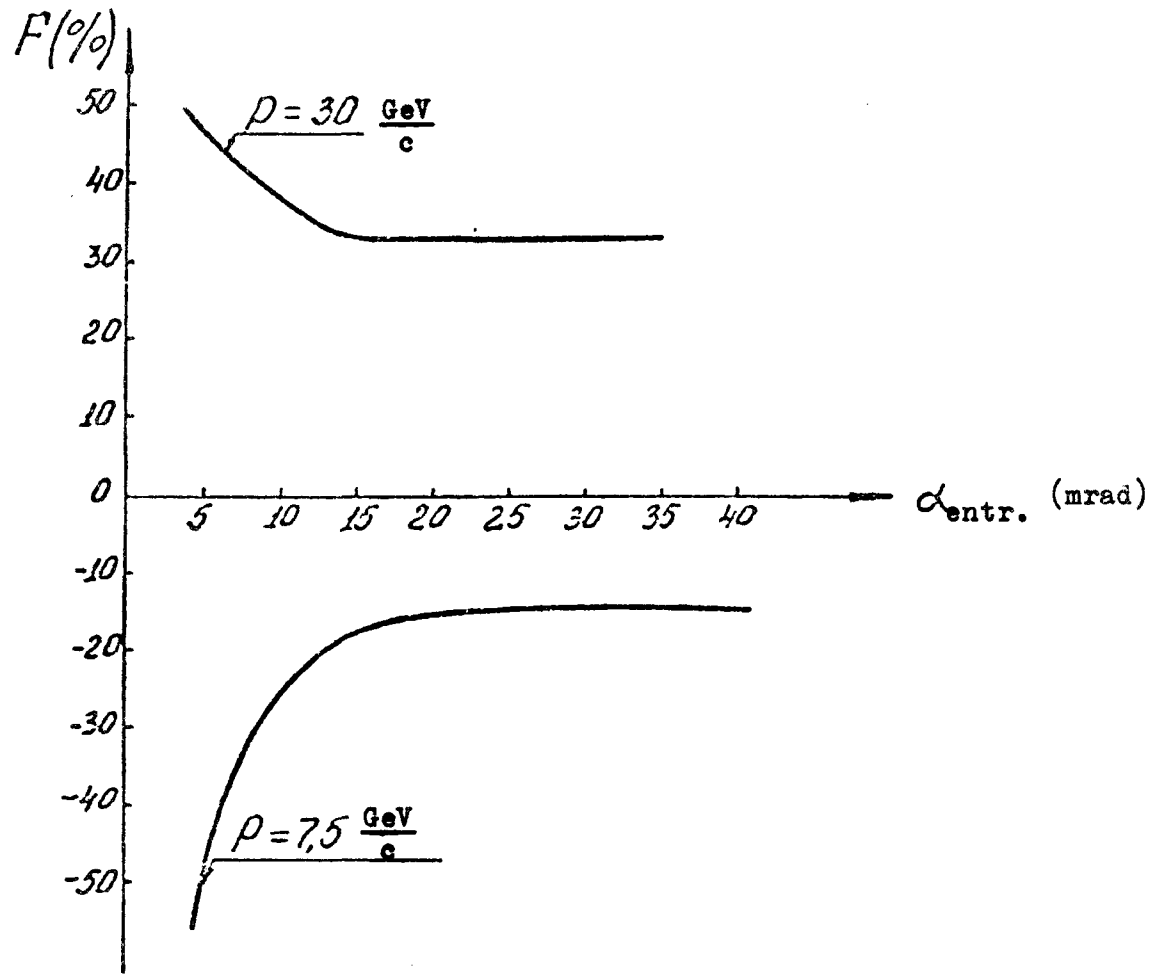

Fig. 21. Effect of the neck on the focussing - entrance angle dependence.

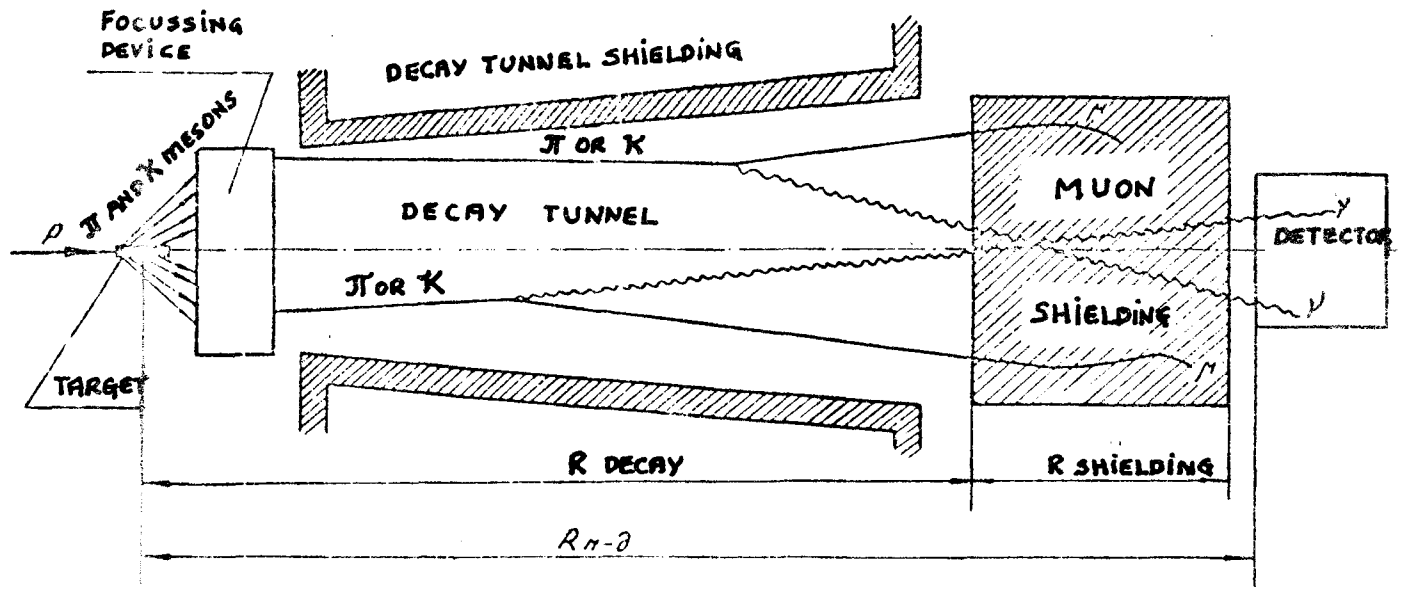

Fig. 22. Block diagram of the device used for producing the neutrino beam.

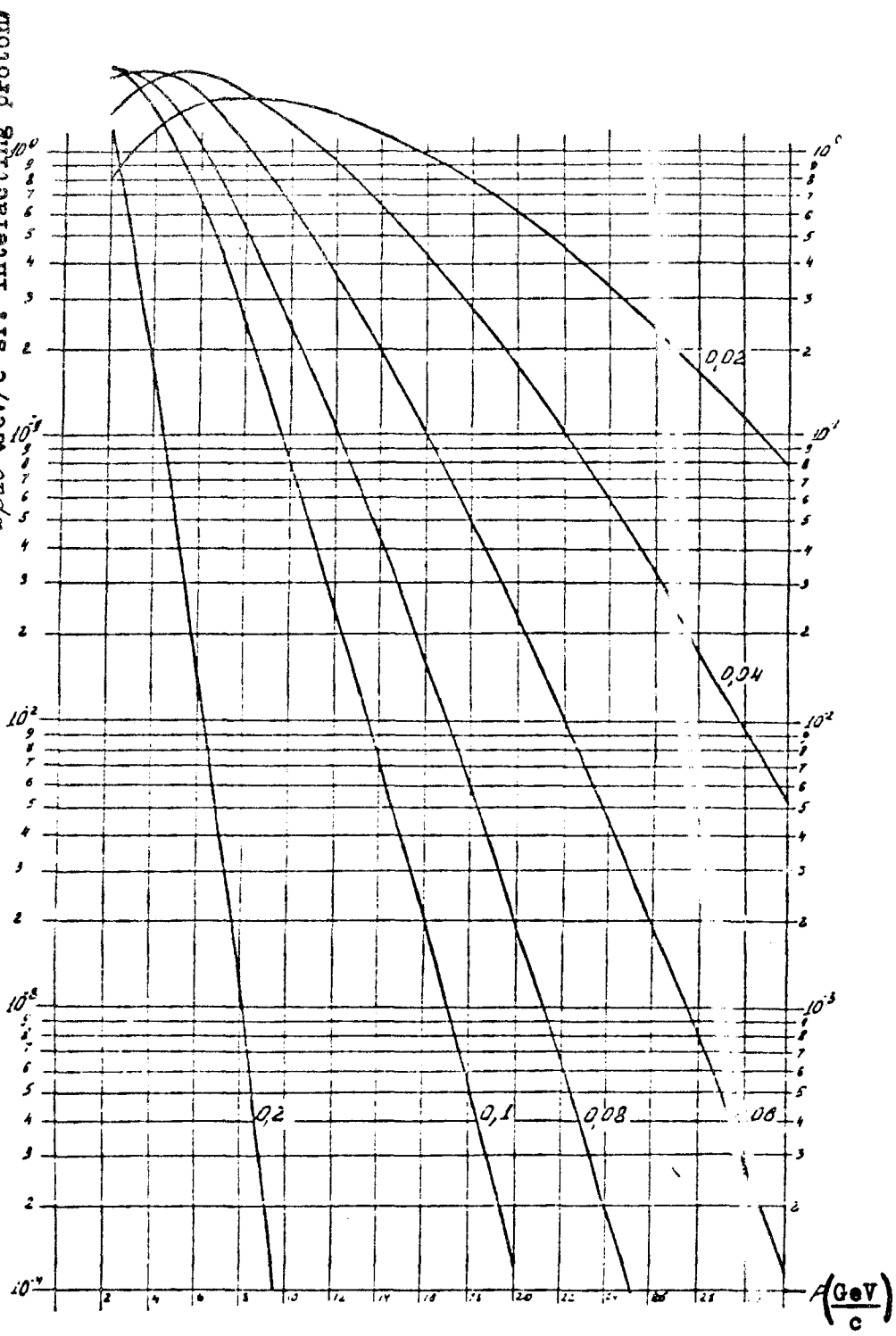

Fig. 23. Differential spectrum of π^+-mesons calculated by the Ranft formula.

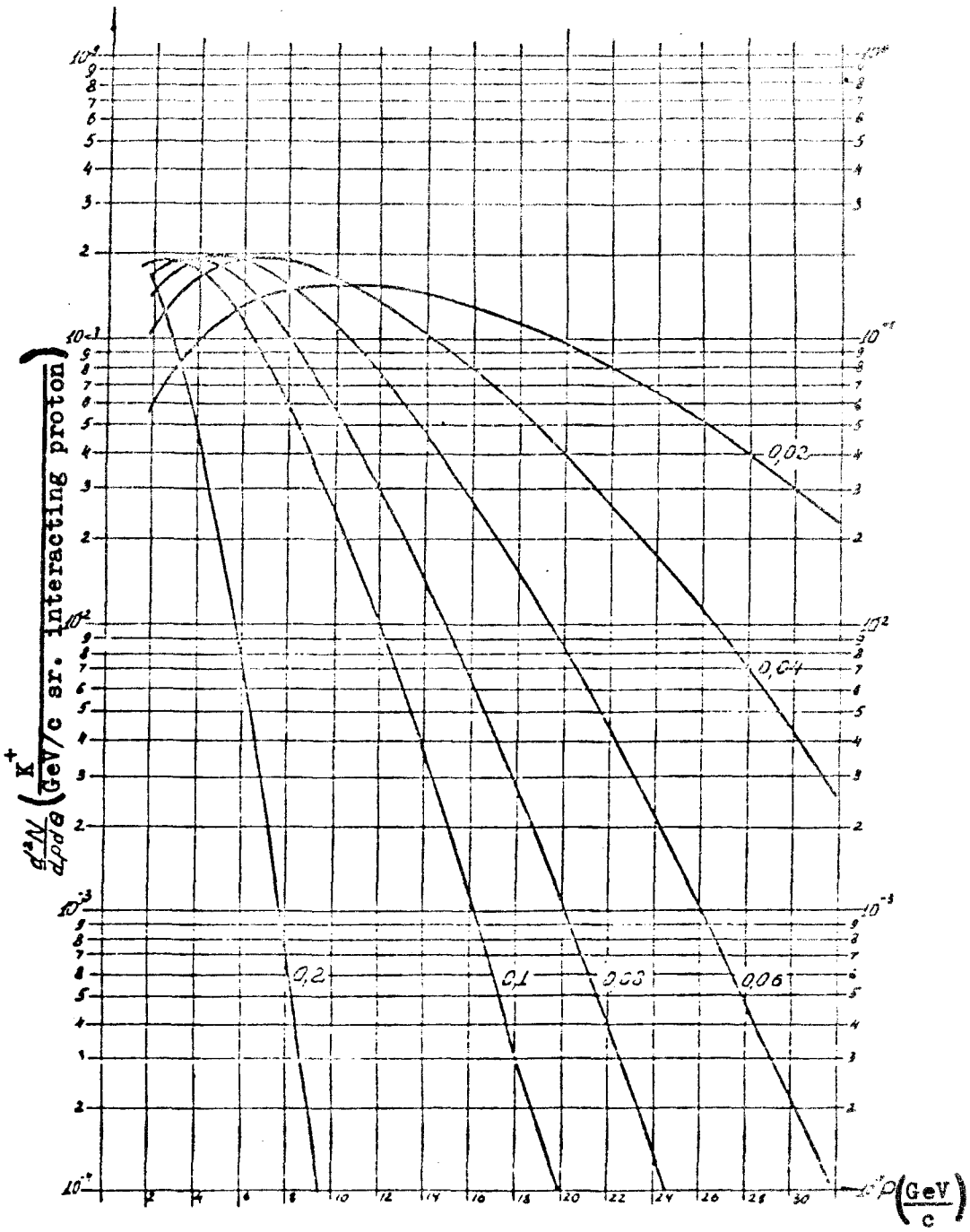

Fig. 24. Differential spectrum of K mesons, calculated by the Ranft formula.

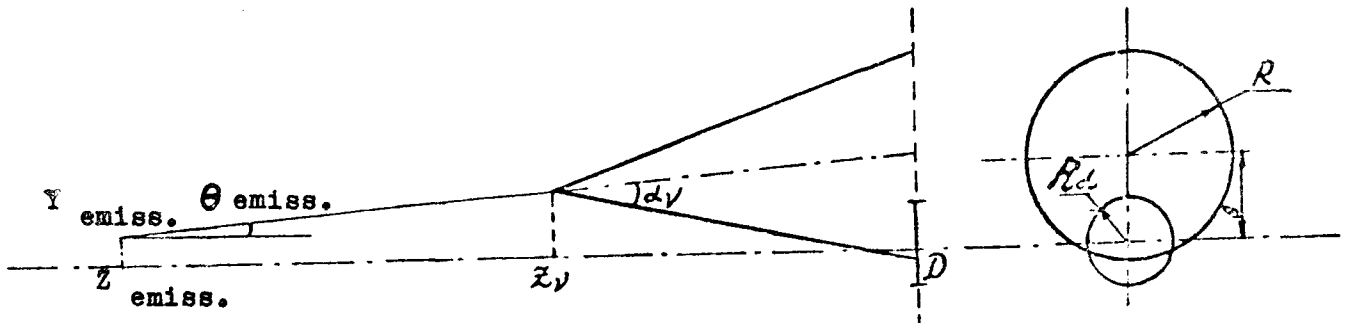

Fig. 25. Probability of a neutrino hitting the detector.
$Y_{emiss.}$ and $Z_{emiss.}$ are the co-ordinates of the point at which the meson leaves the focussing system, $\theta_{emiss.}$ is the angle at which the meson leaves the system, Z_ν is the distance between the meson production and decay points and α_ν is the neutrino's escape angle.

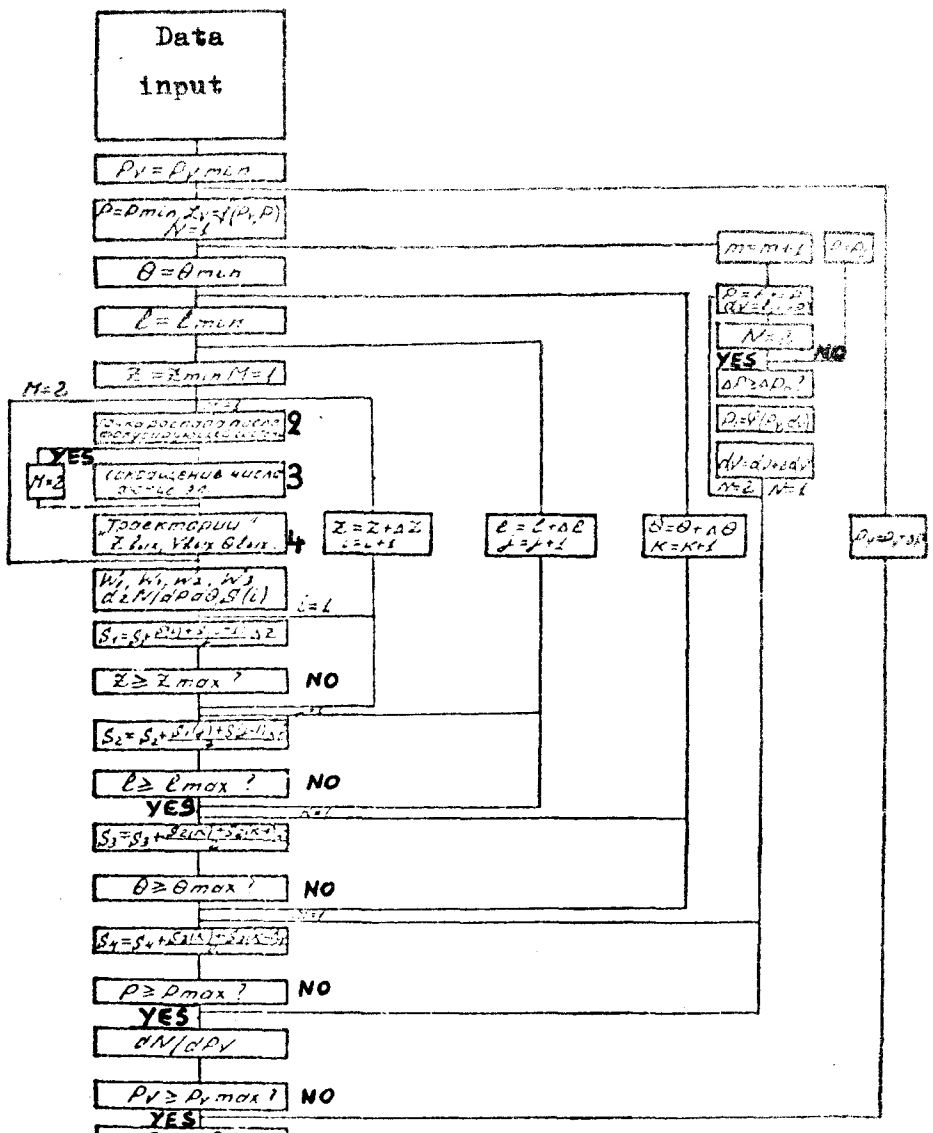

Fig. 26. Lay-out of the program for calculating the neutrino spectrum.
Key: 2 - Decay point after focussing system
3 - Reduction of number of focussing units
4 - "Trajectories" - $Z_{emiss.}$, $Y_{emiss.}$, $\Theta_{emiss.}$

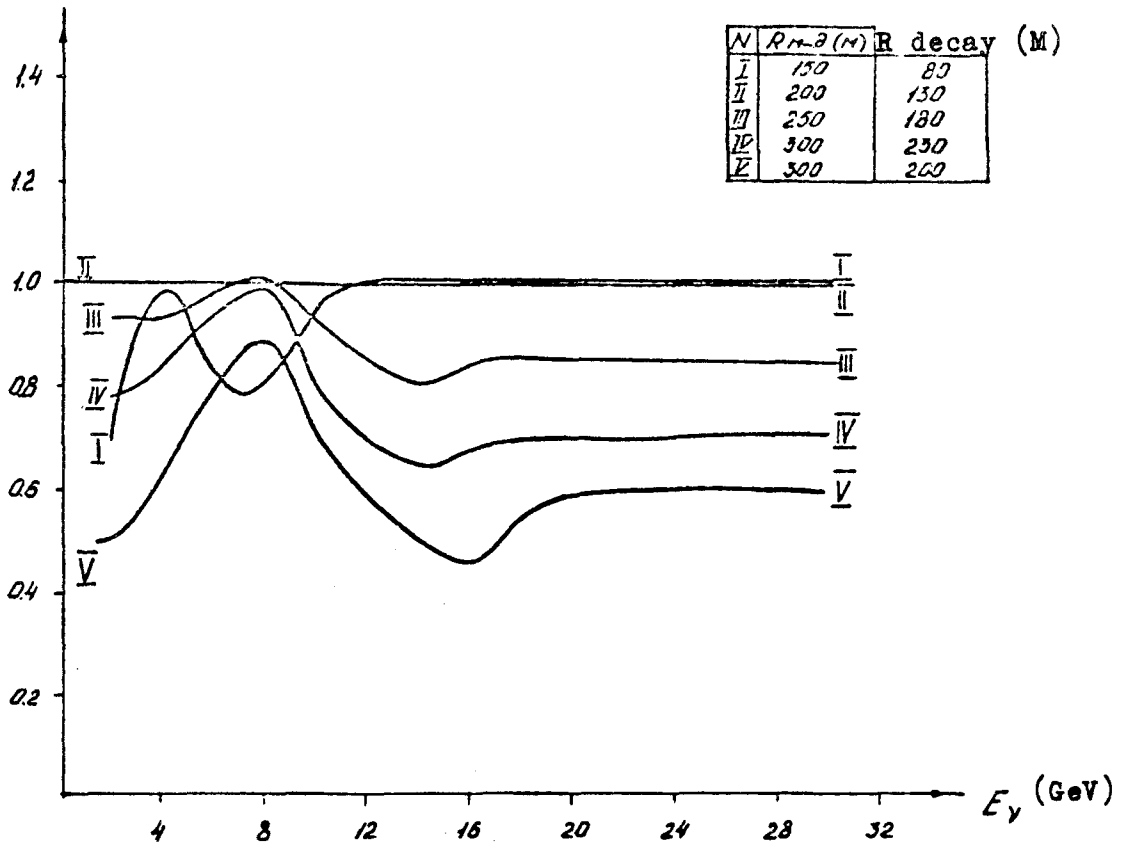

Fig. 27. Relative values of a neutrino spectrum in units of spectrum II. Detector radius 0,5 m.

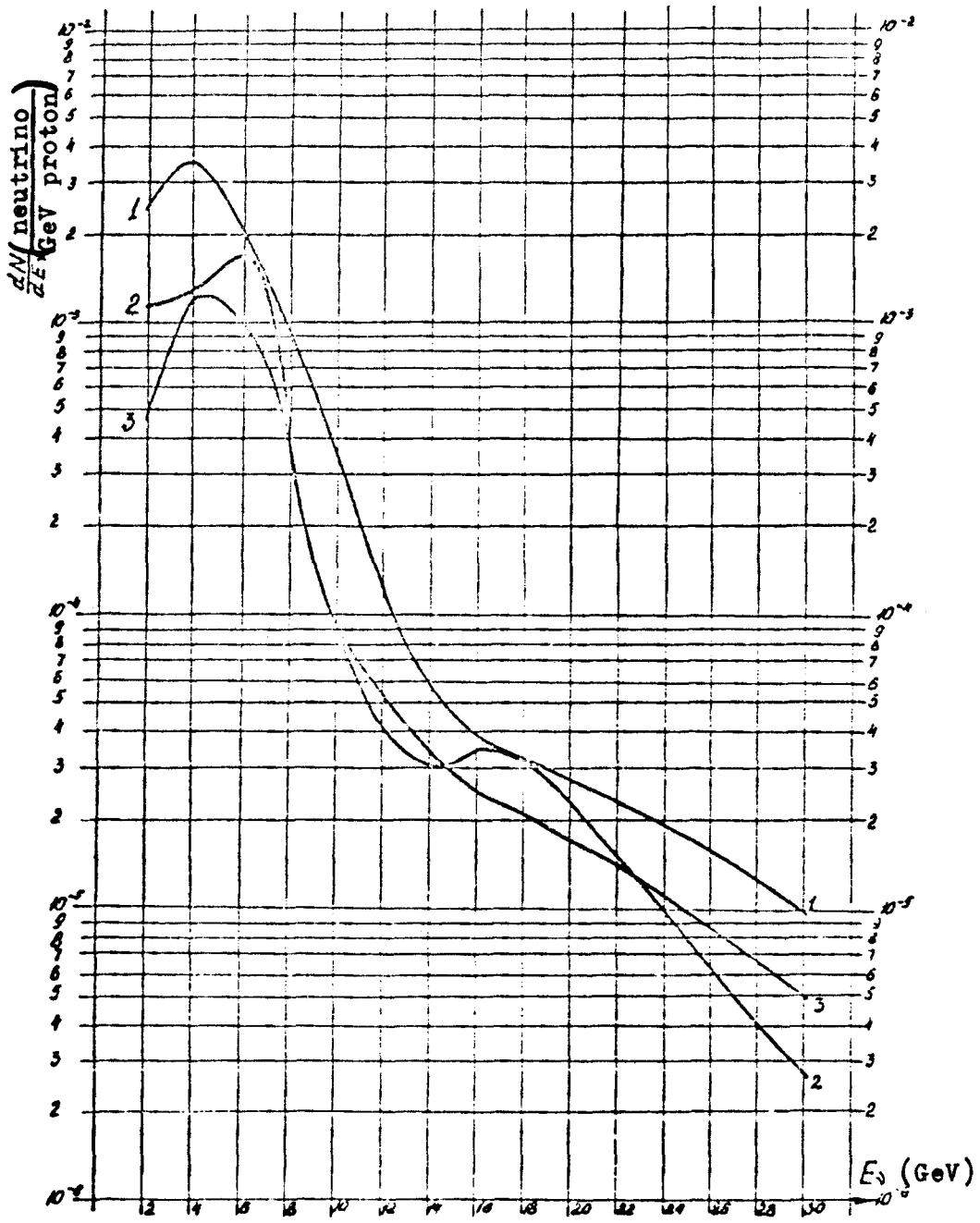

Fig. 28. Neutrino spectra at R_∂ = 0,5 m; $R_{M-\partial}$ = 200 m.
1 - ideal meson focussing; 2 - focussing by parabolic lenses; 3 - focussing by the horn + reflector system (Italian project).

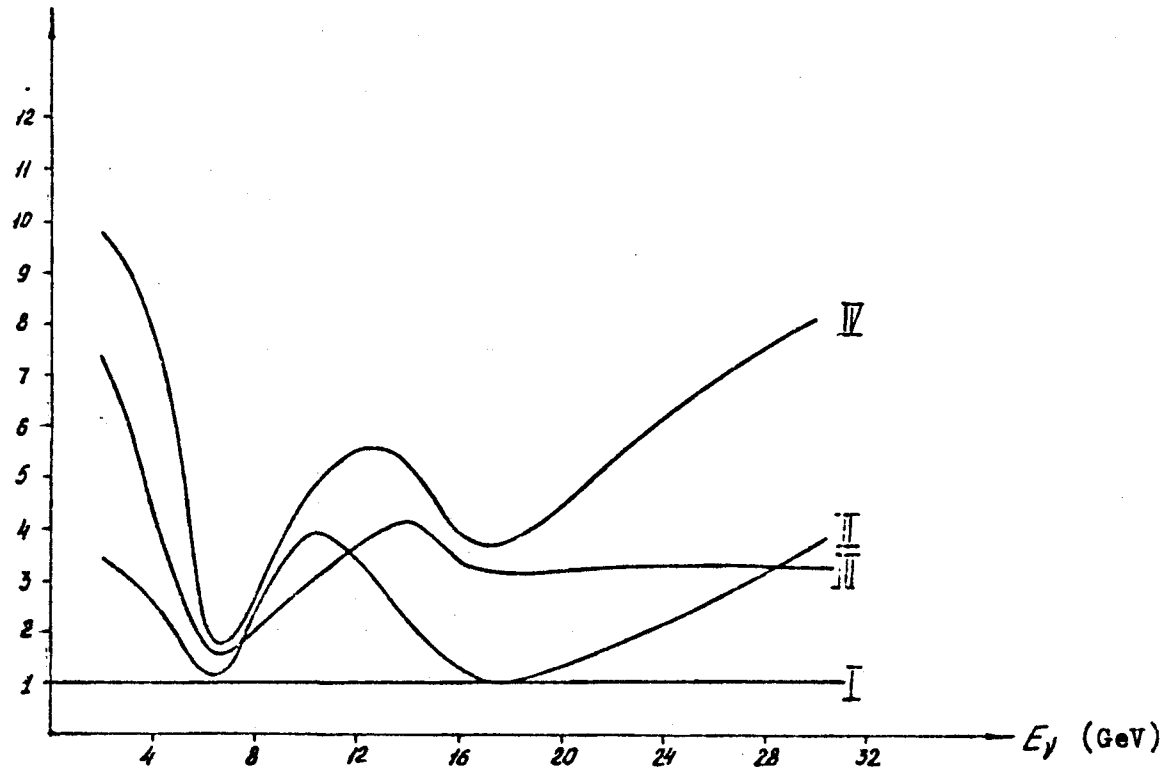

Fig. 29. Relative values of neutrino spectra in units of spectrum 1. R_{m-} ∂ = 200 m. Curve I - actual focussing. Curve II - ideal focussing for R ∂ = 0.5 m. Curve III, IV - similar curves for R ∂ = 1.0 m.

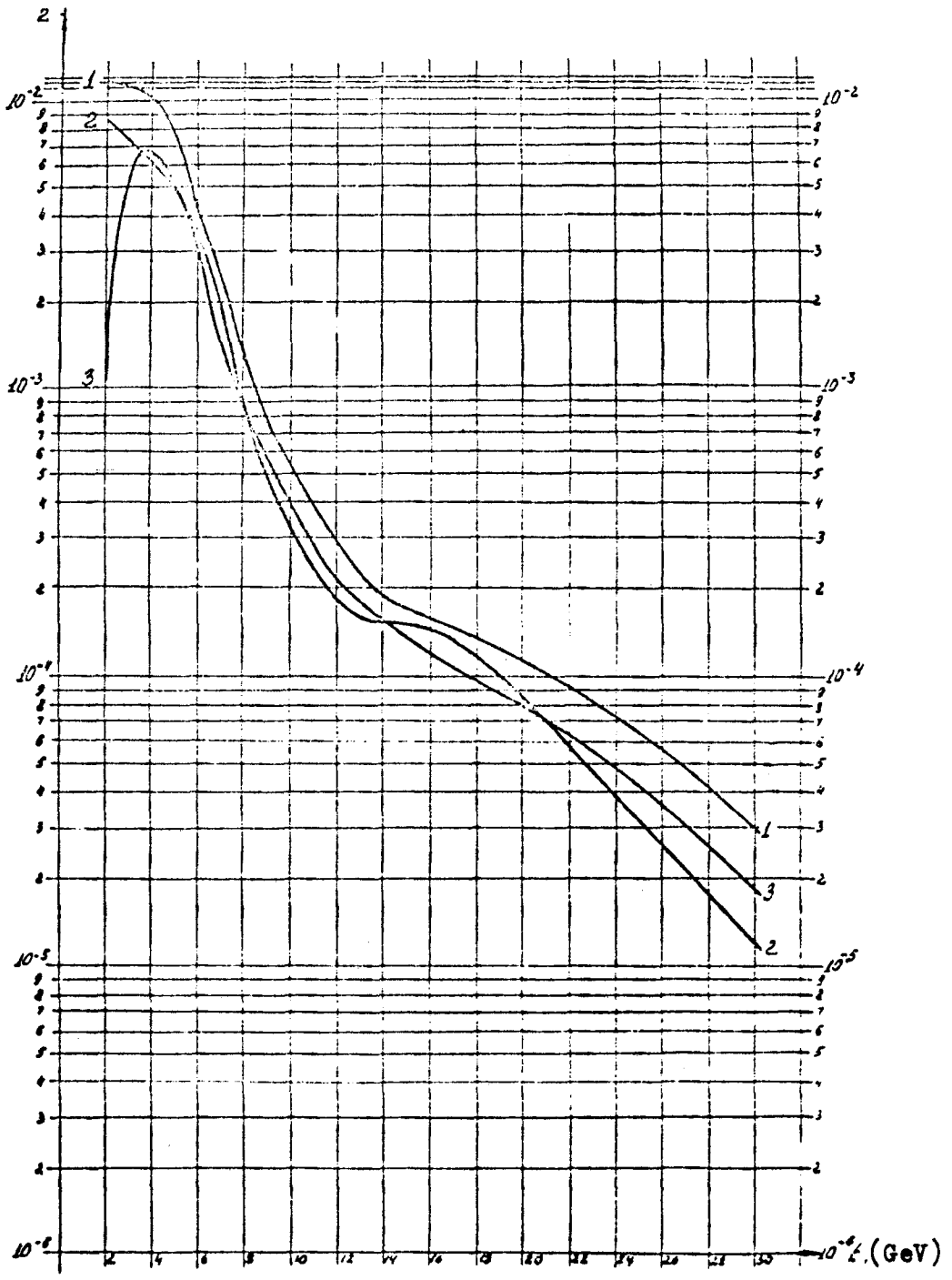

Fig. 30. Neutrino spectra at $R_{\partial} = 1{,}0$ m; $R_{M-\partial} = 200$ m.
1 - ideal focussing; 2 - focussing by parabolic lenses; 3 - focussing by horn + reflector system.